System Performance Analysis Under Correlated Shadow Fading

DISSERTATION

Submitted in Partial Fulfillment of

the Requirements for

the Degree of

DOCTOR OF PHILOSOPHY (Electrical Engineering)

at the

NEW YORK UNIVERSITY
TANDON SCHOOL OF ENGINEERING

by

Tingting Lu

May 2017

System Performance Analysis Under Correlated Shadow Fading

DISSERTATION

Submitted in Partial Fulfillment of

the Requirements for

the Degree of

DOCTOR OF PHILOSOPHY (Electrical Engineering)

at the

NEW YORK UNIVERSITY

TANDON SCHOOL OF ENGINEERING

by

Tingting Lu

May 2017

Approved:

_____

Department Chair Signature

_____

Date

University ID: N19324363
Net ID: tl984

Approved by the Guidance Committee:

Major: Electrical Engineering

Shivendra S. Panwar
Professor
Electrical and Computer Engineering

Date

Elza Erkip
Professor
Electrical and Computer Engineering

Date

Sundeep Rangan
Associate Professor
Electrical and Computer Engineering

Date

Henry Bertoni
Professor
Electrical and Computer Engineering

Date

VITA

Sanjay Goyal was born ******.

To ******.

ACKNOWLEDGEMENT

First and foremost I would like to thank *******

ABSTRACT

TITLE OF YOUR DISSERTATION

by

Your Name

Advisor: Advisor's Name

Submitted in Partial Fulfillment of the Requirements for
the Degree of Doctor of Philosophy (Electrical Engineering)

September/May/January 20**

List of Publications

1. **Tingting Lu**, co-authors, "paper Title," in *Conference name*, Month Year, pp. **.

2. *******

3. *******

Contents

List of Figures

List of Tables

Chapter 1

Introduction

1.1 Challenge, Motivation and Our Approach

The remarkable success of cellular wireless communication technologies make it possible for smartphones to be widely used, which generates dramatical demand increase for mobile broadband capacity every year [1–3]. As a result, the conventional cellular bands below 3 GHz are very crowded. With the severe shortage in conventional cellular bands, millimeter wave (mmWave), between 30 and 300 GHz, frequency spectrum has been considered as a key component to address the bandwidth deficiency in the next generation wireless communication network [4–8]. The available spectrum at these higher frequencies can be easily 200 times more than today's cellular allocations that are largely constrained to the prime RF under 3 GHz. Moreover, the small wavelenths of mmWave signals combined with low-power complementary metal-oxide-semiconductor (CMOS) radio-frequency (RF) circuits enable large numbers of miniaturized antennas to be placed in small dimensions. Usage of these multiple antenna systems make it possible to make electrically steerable arrays with very high gain to be fabricated at the the Base

Station (BS) or even in the cellphone [9–12]. These hardware and system advances promise mmWave a bright future.

1.1.1 Next Generation Cellular Network

There are fundamental differences between current cellular communication system and mmWave communication system, in terms of high propagation loss and sensitivity to blockage. Applications running on top of mmWave network will requires low delay and high capacity. With high capacity, mmWave can easily satisfy the capacity demand. Meanwhile, mmWave system makes it more challenging to provide low delay. These characteristics of mmWave channel result in tough challenges to fully exploit its potential. Fading can substantially affect the performance of a wireless communication system. In general, fading can be divided into two categories: large-scale fading and small-scale fading. Small-scale fading is caused by multipath propagation. Large-scale fading, which is also known as shadow fading, is caused by obstacles in the propagation path. Electromagnetic waves have weak ability to diffract around obstacles with a size significantly larger than its wavelength. Currently the frequency used by LTE system has longer wavelength than mmWave. This makes it possible to overcome the shadow fading caused by small size obstacles. High frequency mmWave has small wavelength, which makes it more sensitive to blockage caused by small size obstacles like buildings, trees and even nearby pedestrians or vehicles. Therefore, shadow fading has significant impact on the performance of the next generation wireless communication system. Shadow fading can cause significant received power loss. We can conclude from what we have stated above that mmWave channel can be severely vulnerable to shadowing resulting in outages, rapidly changing channel

conditions and intermittent connectivity.

(before you jump to a detailed shadow model, expand the discussion above by adding due to the low delay required by applications, even though mmWave have very high bandwidth, it shortcoming has to be mitigated. One way to do so is to use multiple BS to provide diversity, and that's why you care about correlated shadow fading. You should also talk about the on-off nature of mmWave links, and why that will affect transport layer, which is why you take TCP as part of your thesis study.)

Shadow fading is an important factor to be considered when analyzing the system performance. In most cases, shadow fading is assumed to be temporally and spatially independent to simplify the analysis of the system performance. Obviously this is not the real scenario, especially for next generation wireless communication network. For mmWave communication networks, the cell size will become mush smaller than current LTE cell size due to high propagation loss **(add citation)**. When cell size becomes comparable with the size of obstacles that cause shadow fading, shadow fading cannot be considered as spatially independent. Due to the aforementioned characteristics of mmWave channel and next generation wireless communication network, this thesis focuses on investigating the system performance under correlated shadow fading. Since there is no consensus on standard mmWave channel, we study the system performance under correlated shadow fading of the legacy cellular spectrum frequency and suggest it can be applied to mmWave channel in the future.

(the following should belongs to your chapter, not introduction)

At first, we choose distance-angle correlation model**(cite)** for shadow fading and investigate the correlated shadow fading problem in a single-cell cellular net-

work. We find that correlated shadow fading could lead to correlated outage and long outage durations. **(With non-correlated shadow model, we can only analysis a snapshot of the system. However, in order to predict application performance over time, such as outage durations, correlated shadow fading model is necessary)**. To mitigate shadow fading and decrease shadow durations, wireless relays are deployed. The performance of three different relay deployments with different relay densities are investigated. Theoretical analysis and simulations of outage performance are compared between different relay placement scenarios. [**?**, **?**]This work illustrate that uniformly spaced relays perform better than the randomly spaced. Single-cell model is not suitable for analyzing next generation wireless communication networks. Therefore, extending the investigation to multi-cell network is necessary. **(why single cell analysis is not suitable? Is it because you believe the future network cannot rely on a single BS since diversity is essential? Explain)**The disadvantage of the distance-angle correlation model is that it scales with cell size when considering denser network. This is not realistic since the obstacle size will not scale with the cell size. **(Don't understand why scale is a bad thing. Are you trying to say the network is denser so cell radius is small? If so, why the distance angle cannot be used? Purely because of complexity)**Due to this feature, we choose to use exponential correlation model when we study multi-cell network.

Exponential correlation model**(cite)** has been widely used by researchers. Considering a single-cell model, exponentially correlated shadow fading can be modeled as a first-order autoregressive process. **(Should add more background before talking details, I still feel such detail should not be in intro section)** Given this feature, a first-order Markov chain model is developed and vali-

dated. The Markov chain model is constructed by partitioning the entire shadow fading range into a finite number of intervals. The state transition matrix of the Markov chain is derived from the joint probability distribution of correlated log-normal shadow fading. Based on the proposed Markov chain model, the frequency and duration of outage near the edge of a single cell can be analyzed. To validate the Markov chain model, correlated Gaussian random fields are simulated to analyze the outage frequency and durations due to correlated shadow fading. Comparing the simulation results with the Markov chain model results, we conclude **(Don't show your results, intro should be a place to tell people why the things you are going to talk about is important, and how you plan to do it, instead of results.)** that the proposed Markov chain model is an efficient way to describe the channel variations, and the user experienced outage behavior of the channel. This Markov chain model can not be extended to multi-cell system because of the existing of interference from other base stations (BSs). **(Don't understand previous sentence)** To further investigate the performance of multi-cell system, we run simulation for different BS densities. Two scenarios are investigated: MU connecting to the nearest BS and MU connecting to the BS with strongest signal. We calculate signal-to-noise-and-interference ratio (SINR) for the mobile user (MU) with regard to different scenarios. Outage probability and outage duration can be generated from the SINR result. We conclude **(no "conclude")** that increasing BS densities can decrease outage probability when MU is connected to the nearest BS. Outage duration will decrease when increasing the BS density in both cases.

(Before talking about simulation. Explain why you care about higher layer performance, why TCP will have problem on mmWave channels) In order to investigate application performance, an NS-2 **(?)** based link layer

model is employed. The simulation model is based on an Ethernet channel with high capacity and low delay. We extended the model to allow the physical link to be periodic on-off to mimic the mmWave channel. Existing TCP congestion control protocols are tested on this channel. Both throughputs and the variation of congestion windows are showed with regard to different channel behaviors. A data-driven fast congestion prediction algorithm is proposed based on the idea of Explicit Congestion Notification (ECN). This fast congestion prediction algorithm can be utilized to design next generation transport layer protocols.

1.1.2 Correlated Shadow Fading Models

In most cases, shadow fading is modeled as an independent log-normal distribution [13] with a standard deviation derived from empirical measurements. An independent log-normal shadowing model is used widely when shadow fading cannot be ignored. But this model fails to capture the spatial correlations in shadow fading, which has been proved to be not negligible in [14], [15] and [16]. In [17], the author elaborated several models for correlated shadow fading, investigated their feasibility and presented the physical plausibility of each model. Correlations can be divided into two categories: autocorrelation and cross-correlation as in Figure 1.1. Autocorrelation is the correlation between two receivers receiving signal from the same transmitting node. Cross-correlation considers two transmitting nodes transmitted to the same receiver. Autocorrelation and cross-correlation are symmetric in mathematical sense and can be investigated in the same manner.

Autocorrelation and cross-correlation models can be described as in Figure 1.2. There are N points $Y_1, \cdots, Y_N$. S_i is the logarithm of the power attenuation due to shadowing on each path $\vec{r_i}$. $\mathbb{E}\{S_i\} = 0$ since shadow fading has correlated

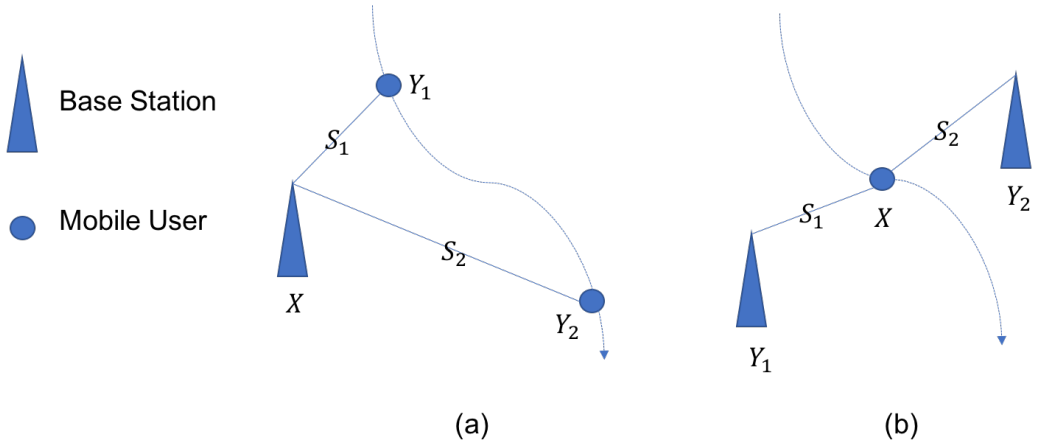

Figure 1.1: (a) Shadowing autocorrelation for a mobile user, (b) Shadowing cross-correlation for a mobile user

log-normal distribution. The log-variance of shadow fading can be characterized as

$$\sigma_i^2 = \mathbb{VAR}\{S_i\} = \sigma_S^2(\vec{r_i}) \tag{1.1}$$

This variance is considered as constant after a certain distance [18].

The correlation coefficients can be defined as

$$\begin{aligned} \rho_{i,j} &= \mathbb{E}\{S_i S_j\}/\sigma_i \sigma_j = h(\vec{r_i}, \vec{r_j}), i \neq j \\ \rho_{i,i} &= 1. \end{aligned} \tag{1.2}$$

The following properties will be held:

- $-1 \leq h(\vec{r_i}, \vec{r_j}) \leq 1$
- $h(\vec{r_i}, \vec{r_j}) = h(\vec{r_j}, \vec{r_i})$

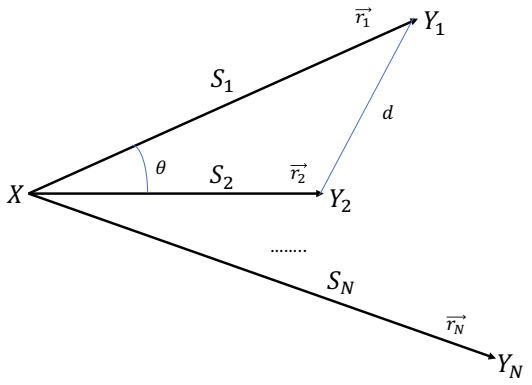

Figure 1.2: Generic geometry of shadowing autocorrelation and cross-correlation

The correlation matrix of $\mathbf{S} = [S_1, \cdots, S_N]$ is:

$$\mathbf{K} = \begin{bmatrix} \sigma_1^2 & \sigma_1\sigma_2\rho_{1,2} & \cdots & \sigma_1\sigma_N\rho_{1,N} \\ \sigma_1\sigma_2\rho_{1,2} & \sigma_2^2 & \cdots & \sigma_2\sigma_N\rho_{2,N} \\ \vdots & \ddots & \ddots & \vdots \\ \sigma_1\sigma_N\rho_{1,N} & \sigma_2\sigma_N\rho_{2,N} & \cdots & 1 \end{bmatrix}. \tag{1.3}$$

For $\mathbf{K}$ to be a valid covariance matrix, it is necessary that $\mathbf{K}$ is positive semidefinite(psd).

By grouping the measurements along one variable in several ways, h can be expressed as a function of a single variable in the following three forms:

- absolute distance (between Y_1 and Y_2): $d = \|\vec{r_1} - \vec{r_2}\|$.
- angle of arrival separation: $\theta = |\angle\vec{r_1} - \angle\vec{r_2}| \in [0°, 180°]$
- arrival distance ratio (in decibels): $R = |10\log_{10} r_1/r_2| = (10/\ln 10)|\ln r_1 -$

$\ln r_2|$

A correlation model needs to satisfy as many as the following criteria to become a precise model:

- $h(\vec{r_i}, \vec{r_j}) \approx 1$ for $\vec{r_i} \approx \vec{r_j}$.
- $h(\vec{r_i}, \vec{r_j}) \ll 1$ for $\|\vec{r_i} - \vec{r_j}\| \gg 0$.
- h should be a nonincreasing function in θ, R and d.
- h should be nonnegative.
- h should be small for large θ and approach zero for $\theta \approx 180°$, and r_1 and r_2 large.
- Continuity: a small change in $\vec{r_i}$ should result in small change in $h(\vec{r_i}, \vec{r_j})$.
- Correlation should not depend on d only.

Considering the above criteria, the author of [17] recommended a correlated shadow fading model with distance and angle in [19], and provided a fast simulation method to generate the correlated shadowing field. We use this model to analyze single-cell system performance and discuss how cooperative communication can help to mitigate shadow fading.

After investigating the single cell system, we further analyzed multi-cell system performance. The aforementioned distance-angle model cannot be applied to this scenario. The correlation coefficient is a piecewise linear function of θ and R. **(Refer to the equation of the model)** When the cell size scales, θ and R remain the same, which means the correlation between two different positions also scales. Since the size of obstacles which generate shadow fading does not

change with cell size, this model violate the physical characteristics of shadow fading. Exponentially correlated shadow fading is the most widely used model. To investigate the multi-cell system performance with correlated shadow fading, we choose the exponential correlation model. Exponential correlation model can be modeled as a Markov chain model in the single-cell case. This Markov model can be used to simplify the analysis of system performance. However, this Markov model cannot be used to analyze the performance of multi-cell system due to the existing of interference. Simulations are run to study the outage probability and outage duration of the multi-cell system given different network topologies.

1.1.3 Transmission Control Protocol (TCP)

TCP is the transport layer protocol that provides reliable connection-oriented and in-order delivery service to applications [20]. TCP uses error control, flow control and congestion control to achieve this. When incoming traffic demand to the network exceeds its capacity, congestion happens and propagates to other connected networks. Congestions in network can generate long delay and high packet loss rate. Due to fading, mmWave cellular network might be unstable and switching between Line-Of-Sight (LOS) and Non-Line-Of-Sight (NLOS) states frequently, which results in large variations in data rate. This behavior determines that mmWave cellular network is prone to congestion. Therefore, design an efficient congestion control protocol is necessary for next generation wireless communication network. There are two points to implement congestion control: end-to-end TCP congestion control and queuing discipline in the routers inside the network.**(Give reference)** In this thesis, we will focus on end-to-end TCP congestion control. Legacy TCP uses slow start, congestion avoidance, and fast

retransmit/fast recovery to adapt to congestion in the routers. The sender maintains two variables for congestion control: a congestion window size (*cwnd*), which upper bounds the sender rate, and a slow start threshold (*ssthresh*), which determines how the sender rate is increased. Initially, *cwnd* increases exponentially until it reaches *ssthresh*. After that, *cwnd* increases roughly linearly. When congestion occurs, *cwnd* is reduced to 1 segment to avoid segment loss.

TCP relies on implicit signals received from receiver or timer time out to learn the state of the network. There are two ways in which TCP can detect packet loss:

- Timer time out: For each sent TCP segment, the sender expects to receive an acknowledgement (ACK) from the receiver within some period of time. If the ACK to a particular segment is not received by the sender before timer time out, the segment is considered to be lost.

- Duplicated ACKs: If the receiver received out of order data segment, it cannot acknowledge the out of order segment. Instead, it will acknowledge the last contiguous segment it has received prior to the lost segment. Upon the reception of the duplicate ACKs, the sender is informed about the lost of the segment.

Both the above methods requires sender to wait for a period of time before start retransmission (timer time out or duplicate ACKs). **(Say one or two sentences about why TCP works for regular network, then compare that to mmWave system, and make the conclusion that it won't work for mmWave. One example is that it is for stable link and only variation is congestion, however, mmwave is on-off, TCP is not for link with lots of lost packet, which is the case for mmWave. Basically, expand the**

following paragraph and make a comparison to predict why TCP fails)

Considering the characteristics of mmWave channel, legacy TCP is not necessary to be a good choice for next generation networks. The slow start will be too conservative for senders to fully utilize the channel capacity. Since low delay mmWave channel switch between LOS and NLOS fast and frequently, time out and duplicate ACKs might not indicate the network condition precisely due to the long waiting time. To investigate the existing TCP performance on mmWave-like channel, we used high capacity **(NS-2 based)** Ethernet channel with periodical on-off behavior to mimic the mmWave channel. TCP throughput of NewReno and Cubic **(references)** are tested on this channel.

There are also some non-TCP congestion control techniques including Random Early Detection (RED), Explicit Congestion Notification (ECN) and so on. After investigating the legacy TCP performance on a mimic mmWave channel, we proposed an end-user TCP congestion prediction algorithm based on ECN. The key idea of ECN is to mark packets as congestion experienced when the routing queue is longer than a threshold instead of dropping them. When the receiver receives the marked packet, it response with a marked ACK to inform the sender that congestion may happen in the router. TCP senders can adjust their rate of transmission based on its own congestion avoidance algorithm. Inspired by ECN, we proposed a data driven virtual ECN algorithm to predict network congestions without involving routers or receivers.

1.2 Dissertation Outline

This thesis is organized as follows. In Chapter 2, we introduce distance-angle correlated shadow fading model and investigate the system performance of a single

cell cellular network. We explain that the correlated shadow fading could lead to correlated outage and long outage durations. To mitigate the shadow fading, relays are deployed to work cooperatively with the BS. The performance of three different relay deployments with different relay densities are discussed. Theoretical analysis and simulations of outage performance are given to compare between different relay placement scenarios.

In Chapter 3, the most widely used shadow fading correlation model: exponential correlation model is introduced. A Markov chain model is constructed for the spatially exponentially correlated shadow fading. This model can be used to analyze the outage behavior for a single cell system. We demonstrated that a well designed Markov chain model with an appropriate number of states corresponding to the standard deviation of the shadow fading is indeed a powerful tool to study system performance.

In Chapter 4, we extend the system performance analysis under exponentially correlated shadow fading from single-cell system to multi-cell system. We compare two different BS layout: Grid Layout and Random Layout and conclude that Grid Layout performs better than Random Layout. System performance are investigated in terms of outage probability and outage duration given different BS density and connection strategies.

In Chapter 5, we investigate the performance of legacy TCP on mimic mmWave channel. The result suggests that legacy TCP is not well designed for next generation network. We proposed a data driven machine learning congestion detection algorithm. The algorithm can predict network congestion with high precision when network topology does not change dramatically. Future fast reacting congestion control algorithm can be designed based on this algorithm.

Chapter 6 concludes the thesis and discuss some future research directions.

Chapter 2

Cooperative Communication to Mitigate Correlated Shadow Fading

In a cellular network, connections between the Base Station (BS) and Mobile Stations (MS) may fail when the channel is in a deep fade. Shadow fading is large-scale fading which can cause significant received power loss for a wide area. This will lead to lost connections and/or packet loss which is harmful to mobile users, especially to those who are using real-time applications such as video conferencing. Cooperative communication is an efficient way to reduce outage and provide better Quality of Service (QoS) support for delay sensitive applications. A third station, which is often referred as a relay, can be used to forward signals between the BS and the MS. This chapter focuses on a study of the performance of relay deployments under correlated shadow fading. We consider the downlink direction in a single cell deployment, for which the shadowing effect is modeled as an angle and distance based correlated shadowing. The received signal-to-noise ratio (SNR) is then calculated by assuming jointly Gaussian shadow fading at the MS. Simulation results show channel variations over time with fixed user speed under

different relay deployments. These results demonstrate that a modest number of relays can improve the performance of real-time applications significantly.

2.1 Background

In a cellular communication system, the connection between the base station and a mobile station may be dropped when the mobile enters a deeply shadowed area. Shadow fading due to buildings, mountains or even trees significantly reduces the power of the received signal. In most cases, shadow fading is assumed to be temporally and spatially independent [21]. In [22] and [23], the effects of correlated shadowing in connectivity is demonstrated, which indicates that reliable connectivity will be much more difficult to maintain than indicated by independent fading shadow models. In a cellular system, for a downlink, the transmitter is a Base Station (BS) and the receiver is a Mobile Station (MS). For real-time applications (e.g. video conferencing), which require high bandwidth and are delay sensitive, the session may get dropped. In general, within a speed limit, the faster the MS moves, the more frequently the channel condition changes and the higher the connection loss frequency. The focus of this chapter is to study channel variations due to correlated shadow fading, and provide a solution to reduce the frequency and duration of dropped connections by employing relays when the MS is moving.

Cooperative communication has been proven to be an efficient way to mitigate fast fading and increase the robustness of data connections [24, 25]. However, cooperative communication can also efficiently maintain the connection whenever the channel condition experiences a sudden deterioration due to shadow fading by switching to different relays. Figure 2.1 is an example of cooperative commu-

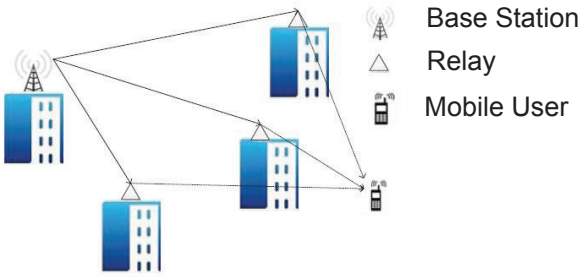

Figure 2.1: Cooperative Communication Example

nication where relays and BS are placed on the top of buildings. In this case, when the MS moves to the area behind a tall building, with a high probability the signal transmitted from the BS will be obstructed by the building, and consequently the MS will encounter deep shadow fading. The channel between BS and MS will degrade and data rate will drop suddenly. In the worst case scenario, the connection with the BS may be totally lost. To combat this effect and enhance the signal received by the MS in this case, relays can be deployed on the top of tall buildings to relay the signals from the BS to MS to maintain good channel conditions between the BS and MS.

Cooperative communication has been a topic of research for several years. Madan et al. [26] studied multi-user spatial diversity in a shadow-fading environment. Other work [27–29], studied relay selection and cooperative relaying over different fading channels in different systems. Patwari et al. [30] studied relay placement in realistic deployments and confirmed that Rayleigh fading alone is not an appropriate assumption for evaluating network performance in a real deployment. In [31, 32], the authors analyzed outage probability and its duration with cooperative relaying. In an 4G-LTE network, which is strongly resilient to multipath fading, shadow fading becomes the most important fading factor [21]. Given the presence of relays, the channel variation experienced by an MS in an en-

vironment with correlated shadow fading is still an open problem. In this chapter, we analyze this problem in a single cell, and give insights on how relays could mitigate shadow fading. We will derive the critical relay density that can guarantee a certain QoS between the BS and an MS.

In most cases, shadow fading is modeled as an independent log-normal distribution [13] with a standard deviation derived from empirical measurements. An independent log-normal shadowing model is used widely when shadow fading cannot be ignored. In the log-normal shadowing model, the path loss ψ is assumed random, with a log-normal distribution given by

$$p(\psi) = \frac{\xi}{\sqrt{2\pi}\sigma_{\psi_{dB}}\psi} exp[-\frac{(10\log_{10}\psi - \mu_{\psi_{dB}})^2}{2\sigma^2_{\psi_{dB}}}], \psi > 0, \tag{2.1}$$

where $\xi = 10/\ln 10$, $\mu_{\psi_{dB}}$ is the mean of $\psi_{dB} = 10\log_{10}\psi$ and $\sigma_{\psi_{dB}}$ is the standard deviation of ψ_{dB}. The distribution of the dB value of ψ is Gaussian with mean $\mu_{\psi_{dB}}$, standard deviation $\sigma_{\psi_{dB}}$ and is given by:

$$p(\psi_{dB}) = \frac{1}{\sqrt{2\pi}\sigma_{\psi_{dB}}} exp[-\frac{(\psi_{dB} - \mu_{\psi_{dB})^2}}{2\sigma^2_{\psi_{dB}}}]. \tag{2.2}$$

The above model fails to capture the spatial correlations in shadow fading. Empirical measurements show that shadowing has significant correlations in realistic scenarios that can affect system performance [14]. Considering the distribution of obstructions and the speed of the MS, a realistic channel propagation model should incorporate correlated shadow fading. Szyszkowicz et al. [17] presented a review and analysis of the feasibility of different correlated shadowing models.

In cooperative communications, relays help the BS to maintain the connection with the MS. Different cooperative schemes can be used by relays. Typically there

are two schemes: Amplify-and-Forward (AF), Decode-and-Forward (DF) [33]. In the AF mode, relays amplify the noisy signal received from the source and forward to the MS. In the DF mode, relays decode the signal received from the BS, then encode it and forward the coded signals to the MS. In this chapter, we assume that DF scheme is used by relays.

Given a fixed placement of BS and a fixed moving trajectory for the MS, the efficient placement of relays to maintain the connection between BS and MS and the resulting reduction of the MS's outage probability under correlated shadow fading is the main focus of this chapter. The key contributions of this chapter are summarized below.

- An analysis of the relationship between correlated shadow fading and correlated outage events.
- Show how relays help mitigate correlated shadow fading. Correlated outage fields with and without relaying are given and compared.
- Analyze the performance of three different relay deployment schemes with different relay densities. The performance includes computing the best channel gain and the resulting change in outage probabilities. We also compare the advantages and disadvantages of different relay deployments.

The chapter is organized as follows: Section 2.2 presents the correlated shadow fading model that is used in this chapter and the resultant correlated outage. Section 2.3 presents the system model with three different relay deployments. Section 2.4 gives theoretical analysis of how relays mitigate shadow fading and reduce outage probability. Section 2.5 presents the simulation setup and analyzes the simulation results of different relay deployments. Section 2.6 summarizes the chapter.

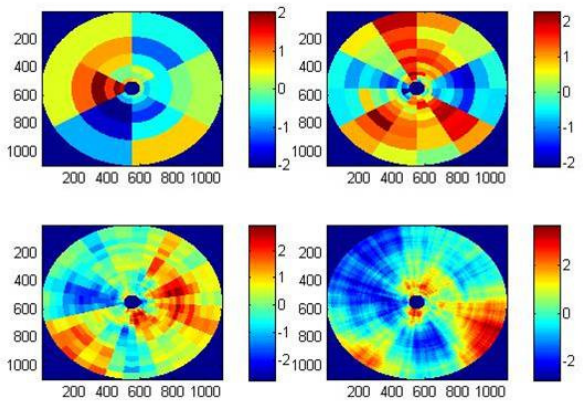

Figure 2.2: Correlated Shadowing Fields for Increasing Resolutions (The disk area is the generated correlated shadowing field and the color of the areas refers to the normalized standard deviation which is $S_i/\sigma_s(\vec{r_i})$)

2.2 Correlated Shadow Fading

As stated in the introduction, empirical measurements show that there exist different patterns of correlations between the shadowing. The independent log-normal shadow fading model, while very useful for static MS performance analysis, cannot reflect the correlation of shadow fading between different locations. In this section, we will give a brief introduction of shadow fading models, including the model used in this chapter. There is no single mathematical model which captures all different categories of correlation [17]. In this chapter, we use the correlated shadow fading model which incorporates the angular and distance correlations of shadow fading [19]. In [19], the author states that correlation in shadowing is indispensable for the analysis of interference of large networks and gives a time-efficient fast shadowing fields generation algorithm. The algorithm generates a correlated shadowing field $\vec{S}$, which gives shadow fading factor $\vec{s_i}$ for each path $\vec{r_i}$

with a correlation matrix

$$\mathbf{K}_{N\times N} = [\sigma_s(\vec{r_i})\sigma_s(\vec{r_j})h(\vec{r_i}\vec{r_j})], \tag{2.3}$$

where N paths interfere with path $\vec{r_i}$ and $\mathbf{E}\{S_i^2|\vec{r_i}\} = \sigma_s^2(\vec{r_i})$. This model assumes that in the correlation matrix, h is separable with respect to the angle of arrival

$$\theta = |\angle\vec{r_i} - \angle\vec{r_j}| \in [0^\circ, 180^\circ], \tag{2.4}$$

and the arrival distance ratio

$$R = |10\log_{10} r_i/r_j| = \frac{10}{\ln 10}|\ln r_i - \ln r_j|, \tag{2.5}$$

$$h(\vec{r_i}, \vec{r_j}) = max\{1 - \theta/\theta_0, 0\} \cdot max\{1 - R/R_0, 0\}. \tag{2.6}$$

Following the fast shadowing field generation algorithm, we generate shadowing fields with different values of tuneable parameters. The shadowing fields are shown in Figure 2.2 with increasing resolutions. Four circular correlated shadowing fields are generated. The shadowing fields are similar to those generated in [19].

2.2.1 Correlated Outage Field

Given a correlated shadowing field, the outage events at different locations are also correlated. Here we analyze correlated outage events under correlated shadow fading and later give an example. In the spatial correlation of outage events, without considering Rayleigh fading, path loss is considered as constant at a fixed time point. Based on the correlated shadowing field we can generate a correlated outage field. Let G denotes total channel gain, PL denotes path loss,

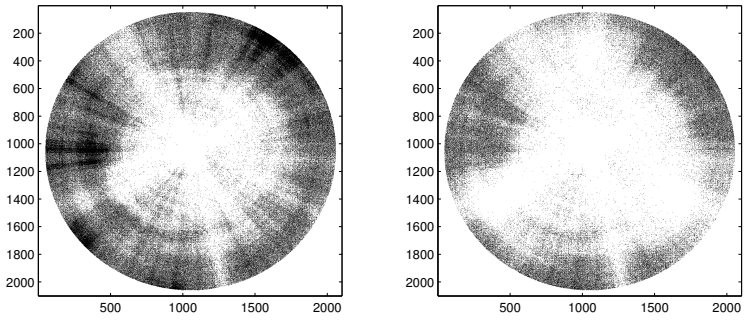

Figure 2.3: Correlated Outage Fields (Dark areas are outage areas while white areas are non-outage areas)

and S denotes shadow fading factor, we then have:

$$G = PL * S \tag{2.7}$$

For two different positions, the correlation coefficient of the two total channel gains is of the following form:

$$\rho_{1,2} = \frac{E[G_1 G_2]}{\sqrt{(Var(G_1)Var(G_2))}}. \tag{2.8}$$

where $G_1 = PL_1 * S_1$ and $G_2 = PL_2 * S_2$. At a fixed time point, temporal correlation is neglected and only spatial correlation is considered, then PL_1, PL_2 can be assumed to be constants, which means that $E[PL_1] = PL_1$, $E[PL_2] = PL_2$. Based on this assumption, we have

$$E[G_1 G_2] = PL_1 PL_2 E[S_1 S_2], \tag{2.9}$$

$$Var(G_1) = PL_1^2 Var(S_1), \tag{2.10}$$

$$Var(G_2) = PL_2^2 Var(S_2), \tag{2.11}$$

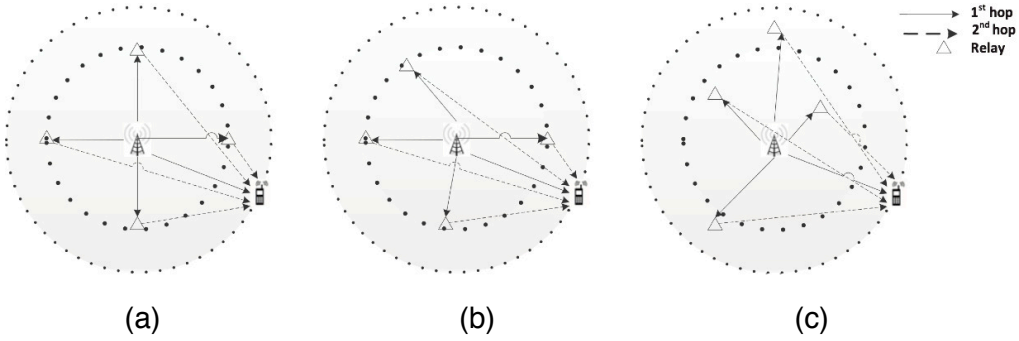

Figure 2.4: System Model and Three Different Relay Placements

Based on (2.9), (2.10) and (2.11), it is straightforward to rewrite (2.8) as:

$$\rho_{1,2} = \frac{E[S_1 S_2]}{\sqrt{Var(S_1)Var(S_2)}} = \rho_{S_1,S_2}. \tag{2.12}$$

The channel gain has a spatial correlation coefficient as shown above. Based on the result above, a correlated channel gain field can be generated. Given a proper threshold γ, the correlated outage field can be generated as in Figure 4.2. On the left, a correlated outage field without relaying is shown while the correlated outage field with relaying (3 relays uniformly placed on a circle near the edge) is given on the right. The black color indicates outage areas. In the next section we will present the methodology that helped us generate the results with relays.

2.3 System Model

Since most of the key aspects of the problem can be studied in a single cell, we consider a single cell cellular deployment, where the BS is located at the center of the cell. Figure 2.4 shows the system model that is used in this chapter. Several relays are placed in the cell and an MS is moving at a particular speed along the circumference at the cell edge. We picked this trajectory since it is the most

challenging path given the combination of shadowing and path loss. We consider three relay deployment modes. From left to right in Figure 2.4, (a) is the mode where relays are placed uniformly on a circle near the cell edge; (b) is relays that are randomly spaced on a circle near the cell edge; (c) is relays placed randomly in the cell. By varying relay densities in the above three different models we can analyze which combination of relay density and relay placement can meet the required QoS.

2.3.1 Cooperative Communication Scheme

In this system, the BS and relays work cooperatively to try to guarantee that the MS has sufficient received power either from the BS or from relays with high probability. There are two main cooperative communication schemes: Amplify-and-Forward, and Decode-and-Forward. In this chapter, we assume that relays use the Decode-and-Forward scheme. The cooperative communication system works in the following manner:

- First Hop: BS broadcasts signals to both relays and MS. If MS receives and decodes the signals transmitted by the BS successfully, there is no need for relays to repeat the transmission. If not, relays which successfully decode the signals will participate in the second hop retransmission. This mode of operation will require some signaling overhead, which is not addressed in this chapter. Relays which cannot decode the received signal successfully, will not participate in the second hop.

- Second Hop: Among all relays which participate in the second hop, the one that has the best channel gain between the relay and MS will be chosen (this can be done by centralized control or using information from pilot signals).

This relay will encode the signals again and send the coded bits to the MS.

The received signal in a link ($S \rightarrow D$) between the source and destination is given by:

$$y_D = G_{SD} x_S + n_D. \tag{2.13}$$

where x_S is the signal transmitted by the source and y_D is the signal received by the destination. $n_D \sim \mathcal{CN}(0, N_0)$ is additive white Gaussian noise. G_{SD} is the channel gain from source to destination including path loss and shadow fading. $\text{SNR} \triangleq P * G_{SD}^2 / N_0$, is the end-to-end received signal-to-noise ratio (SNR) and P is the transmitted power. The destination successfully receives the signals if no outage event happens, i.e., $\log_2(1 + \text{SNR}) \geq R$, where R is the required data rate. From the definition of SNR, no outage event happens as long as $\text{SNR} > \gamma$, where $\gamma = 2^R - 1$. In the first hop, relays that can successfully decode the signals transmitted from the BS is a subset $\mathcal{R}_n$ of N relays defined by:

$$\mathcal{R}_n \triangleq \{i : \log_2(1 + \text{SNR}_{S-i}) \geq R\}, \tag{2.14}$$

where SNR_{S-i} is the received signal-to-noise ratio from BS to relay i and $n \in \{0, 1, \cdots, 2^N\}$. In the first hop, the relay can successfully decode the BS signals if $\text{SNR}_{S-i} > \gamma$. The indices of all relays which are able to successfully decode BS signals form a set $\mathcal{R}_n$. In the second hop, the selected best relay j is the relay in $\mathcal{R}_n$ that has the maximum SNR among all relays in $\mathcal{R}_n$, i.e., $j = \arg\max_{i \in \mathcal{R}_n} \{\text{SNR}_{i-D}\}$, where SNR_{i-D} denotes the SNR from the ith relay to the destination MS. The BS to MS SNR is denoted by SNR_{S-D}. The SNR is determined by distance related path loss and large-scale correlated shadow fading.

2.4 Outage Probability Analysis

Due to the variations of the channel gain caused by shadow fading and path loss of the propagation environment, if the end-to-end channel capacity is below the transmission rate, an outage occurs and the information packets are lost. The outage probability is an important performance measurement of the communication system. In this section, the expression for outage probability is derived.

2.4.1 Outage Probability of the Cooperative Communication System

If an MS cannot directly receive the signal from the BS and none of the relays can decode the BS signal, or if the MS has a bad channel with all relays which successfully decode the BS signal, then an outage event will take place. The probability that an MS cannot receive signals directly from the BS successfully is given below:

$$P_{out_0} = P[\mathrm{SNR}_{S-D} < \gamma], \tag{2.15}$$

Under the assumption that an MS cannot successfully receive signals from the BS, the outage event happens in the first hop if no relay can receive the signal from the BS successfully, which means $\mathcal{R}_0 = \phi$. Based on this assumption we have:

$$P_{out_1} = \max_{i=1,\cdots,N} P[\mathrm{SNR}_{S-i} < \gamma]. \tag{2.16}$$

If the outage does not happen in the first hop, then the outage event may happen in the second hop with probability:

$$P_{out_2} = \sum_{n=1,\cdots,2^N} P[\mathrm{SNR}_{j-D} < \gamma | \mathcal{R}_n] P[\mathcal{R}_n], \tag{2.17}$$

where j is the index of the relay which has the best channel gain between it and the MS. So the outage probability of the system is

$$P_{out_S} = P_{out_0} * (P_{out_1} + (1 - P_{out_1}) * P_{out_2}). \tag{2.18}$$

The probability density function (pdf) of shadow fading S given L correlated fading branches is

$$\begin{aligned} f_{\mathbf{S}}(\mathbf{s}) = & \frac{\lambda^L}{\sqrt{2\pi}|\mathbf{K}_{L\times L}|^{1/2}\prod_{i=1}^{L} s_i} \\ & \cdot \exp(-\frac{1}{2}(10\log_{10}\mathbf{s} - \boldsymbol{\mu})^T \mathbf{K}_{L\times L}^{-1}(10\log_{10}\mathbf{s} - \boldsymbol{\mu})), \end{aligned} \tag{2.19}$$

where $\lambda = 10/\ln 10$ and $\boldsymbol{\mu}$ is the average shadow fading which is normally 0. $\mathbf{K}_{L\times L}$ is the correlation matrix which is defined in (4.5). Let $\theta_i = \frac{10\log_{10} s_i - \mu_i}{\sqrt{2}\sigma_i}$, and doing a change of variables gives us the pdf of $\boldsymbol{\Theta}$ as follows:

$$f_{\boldsymbol{\Theta}}(\grave{}) = \frac{1}{\pi^(L/2)|\boldsymbol{\Sigma}|^{1/2}} \exp(-\boldsymbol{\Theta}^T \boldsymbol{\Sigma}^{-1} \boldsymbol{\Theta}), \tag{2.20}$$

where $\boldsymbol{\Sigma}$ is the correlation coefficient matrix which is

$$\begin{bmatrix} 1 & h_{1,2} & \cdots & h_{1,L} \\ \vdots & \ddots & \ddots & \vdots \\ h_{L,1} & h_{L,2} & \cdots & 1 \end{bmatrix}. \tag{2.21}$$

Since SNR$= PL+S-N_0$ in dB, SNR$>\gamma$ means $S>\gamma-PL+N_0$. Given $\mathcal{S}_0=\phi$, and letting γ_{ai} denote the shadow fading threshold for the ith relay in the ath hop and where $a=0,1,2$, where the 0th hop is the direct transmission from BS to MS, we then have

$$P_{out_1}=\underbrace{\int_{-\infty}^{+\infty}\cdots\int_{-\infty}^{+\infty}}_{i=1,\cdots,N}\prod g_0(\gamma_{1i})f(\mathbf{s_1})d\mathbf{s_1}. \tag{2.22}$$

For $n=1,\cdots,2^N$, the outage probability for the second hop is

$$\begin{aligned}P_{out_2}=\sum_{n=1,\cdots,2^N}&\underbrace{\int_{-\infty}^{+\infty}\cdots\int_{-\infty}^{+\infty}}_{i=1,\cdots,N}\prod g_n(\gamma_{1i})f(\mathbf{s_1})d\mathbf{s_1}\\&\cdot\underbrace{\int_{-\infty}^{+\infty}\cdots\int_{-\infty}^{+\infty}}_{i\in\mathcal{R}_n}\prod g_n(\gamma_{2i})f(\mathbf{s_2})d\mathbf{s_2},\end{aligned} \tag{2.23}$$

where $\mathbf{s_1}$ is the correlated shadow fading in the first hop, $\mathbf{s_2}$ is the correlated shadow fading in the second hop, u is a step function and

$$g_n(\gamma_{ai})=\begin{cases}u(\gamma_{ai}) & i\in\mathcal{R}_n\\ 1-u(\gamma_{ai}) & i\notin\mathcal{R}_n\end{cases}. \tag{2.24}$$

Due to the random nature of propagation environment, P_{out_0} is beyond our control. Therefore, to reduce the outage probability, we need to reduce P_{out_1} and P_{out_2}. Relays at proper positions with sufficient density can reduce the outage probability. Comparing different relay placements and finding the appropriate relay density to guarantee the outage probability requirement is the main issue that we will consider next.

2.5 Simulation and Performance Evaluation

To study which relay placement yields the best system performance i.e., the lowest outage probability for continuous real-time applications that we assume to be running on an MS moving at the cell edge (for the given cooperative communication scheme), we set up simulations and compare performance for different relay placements.

2.5.1 Relay Placement

Different relay placements as shown in Figure 2.4 are studied and compared in this section.

- Mode 1: Relays are uniformly spaced on a circle near the cell edge.
- Mode 2: Relays are randomly spaced on a circle near the cell edge.
- Mode 3: Relays are randomly placed in the cell.

2.5.2 Simulation Configuration

In this chapter, the Okumura-Hata model [34] is used to estimate the path loss. The values of parameters that are used in the simulation are shown in Table 3.1. In Mode 1 and Mode 2, the radius of the circle where relays are placed (near the edge) is $700m$.

2.5.3 Simulation Results and Analysis

In this section, numerical analysis and simulation results are presented. The best channel condition that the user can get from either BS or relay is simulated to demonstrate the improvement of the received signal strength at the MS.

Table 2.1: Simulation Configuration Parameters

Okumura-Hata Model	BS Height: $100m$ Relay Height: $10m$ MS Height: $1.5m$
Correlated Shadow Fading	$R_0 : 6$ $\theta_0 : \pi/3$ $d_{min} : 50m$
Relay Placements	Three Modes with Density: 2,4,6,8,10,12
Cell Size	$R : 1000m$
MS Moving Speed	$v : 10m/s$
Radio Frequency	$f : 900MHz$
BS Transmission Power	$P : 26dbm$
SNR Requirement	$8dB$

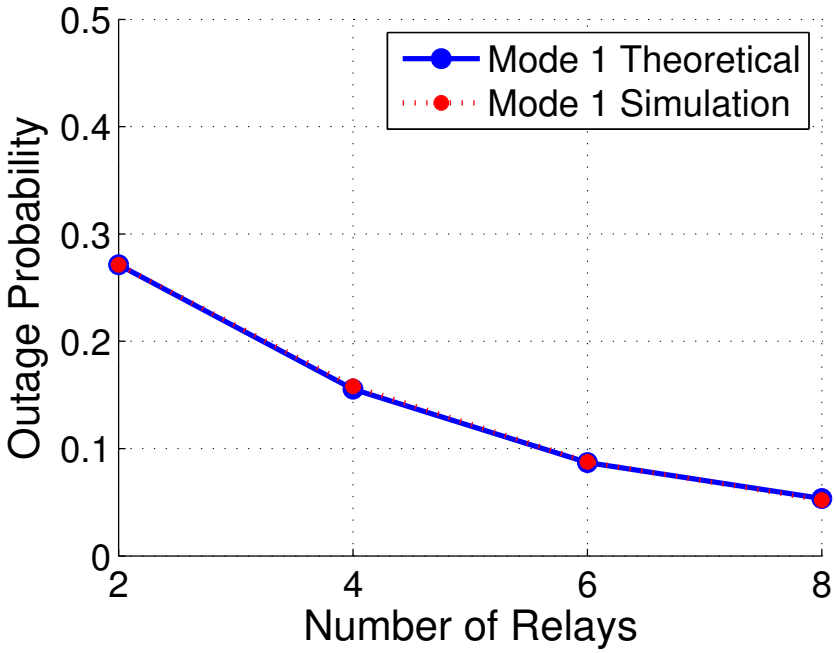

Figure 2.5: Theoretical and Simulated Outage Probability for Mode 1

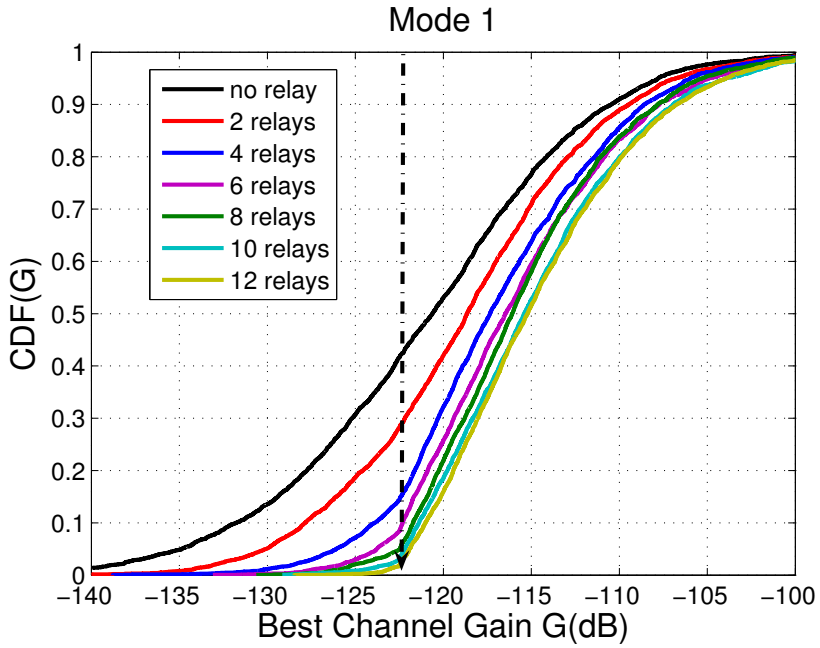

Figure 2.6: Best Channel Condition between MS and BS or Relays of Mode 1 (Dashed arrow demonstrates the channel condition that satisfies the SNR requirement.

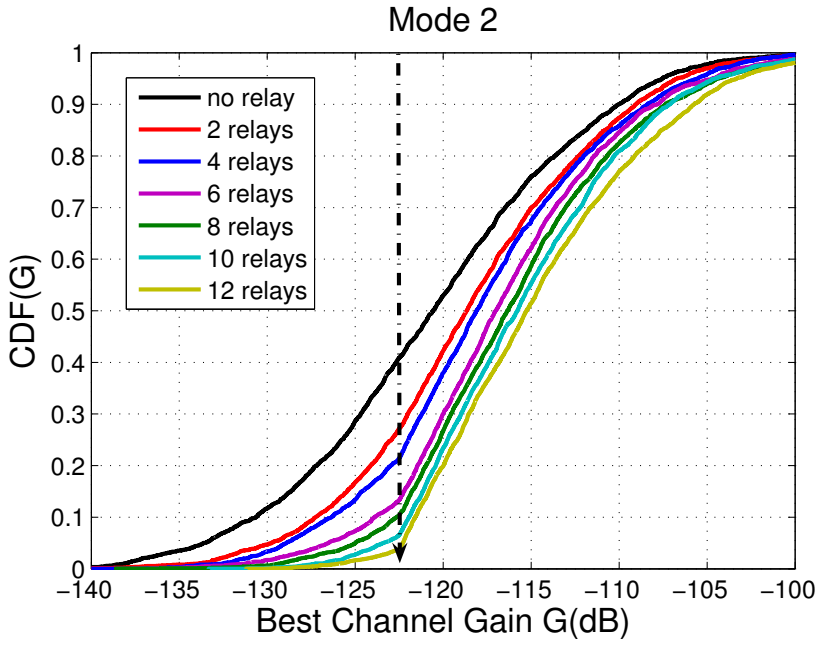

Figure 2.7: Best Channel Condition between MS and BS or Relays of Mode 2 (Dashed arrow demonstrates the channel condition that satisfies the SNR requirement.

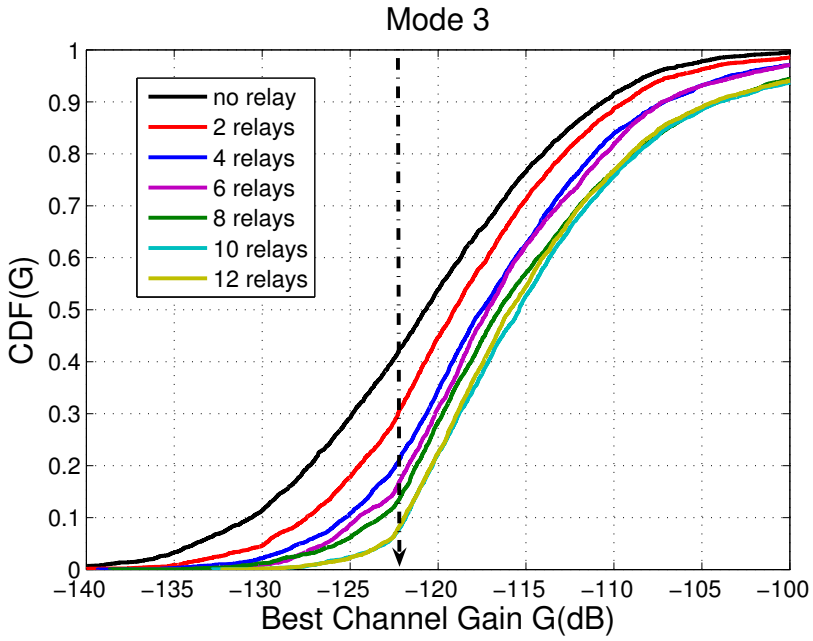

Figure 2.8: Best Channel Condition between MS and BS or Relays of Mode 3 (Dashed arrow demonstrates the channel condition that satisfies the SNR requirement.

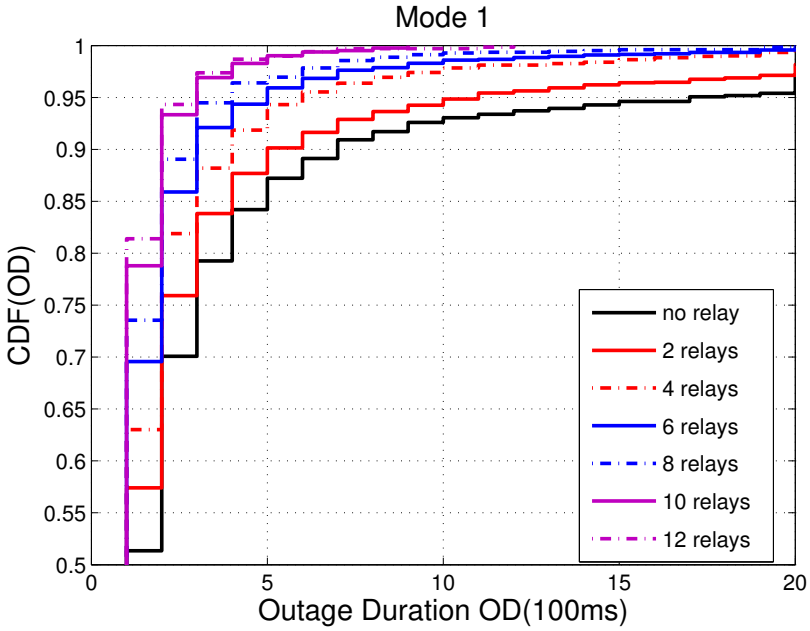

Figure 2.9: Cumulative Distribution Function of Outage Duration of Mode 1 (with Rayleigh fading)

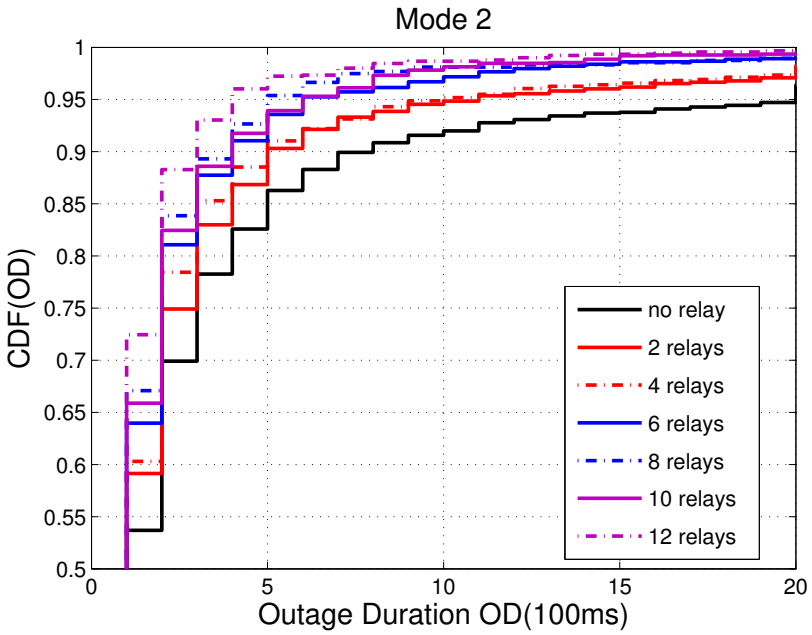

Figure 2.10: Cumulative Distribution Function of Outage Duration of Mode 2 (with Rayleigh fading)

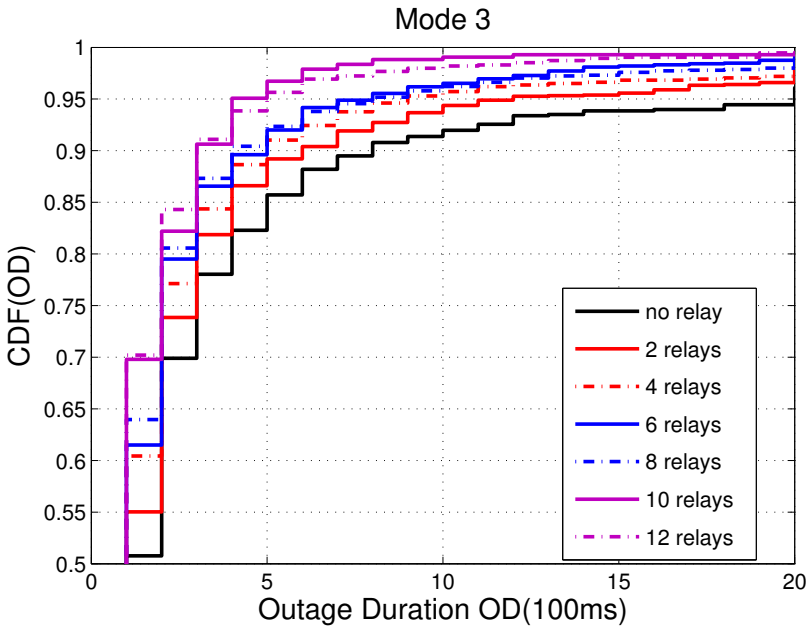

Figure 2.11: Cumulative Distribution Function of Outage Duration of Mode 3 (with Rayleigh fading)

The outage probabilities and durations are shown to indicate the potential user experience improvement when using a real-time application.

First, numerical analysis and simulation results of outage probabilities in Mode 1 is shown in Figure 2.5. The numerical analysis has high computational complexity and is difficult to apply to outage duration analysis. Therefore a simulation is necessary to study the system. Considering the computational complexity, to show that our simulation is validated by analysis, partial comparison between numerical analysis and simulation results is shown in Figure 2.5, which indicates that our simulation code is correct and can be used to study the system.

Second, we simulate the distribution of the best channel gain for the channel between the MS and BS or relays. Figure 2.6, 2.7 and 2.8 plot the distribution of the user channel gain of the three different relay deployment modes and 6 different relay densities. As shown in the figure, the intersection of the dashed arrow and the cumulative distribution function (cdf) plots indicates that as relay density increases, the percentage of outages reduces. The dashed arrow points to $122.5dB$ which is the lowest channel gain to guarantee the SNR to be above $8dB$, in which case 16-QAM with 1/2 code rate will still work. Considering the power constraints, the complexity and cost of placing relays and received SNR requirements, finding a proper relay density is very important. Beyond a certain relay density, increasing the relay density will not give significant additional performance improvement. In all modes, it is shown that relays can mitigate the shadow fading efficiently. For example, in the Mode 1 case, 10 relays can improve the performance by reducing the probability of outage by 40% compared to the no relay case. To compare the results across the three different modes, we take the 10 relay case as an example. For this case, Mode 1 has an outage probability 3% less than Mode 2 and 10% less than Mode 3. In addition, we compare the three different modes from the

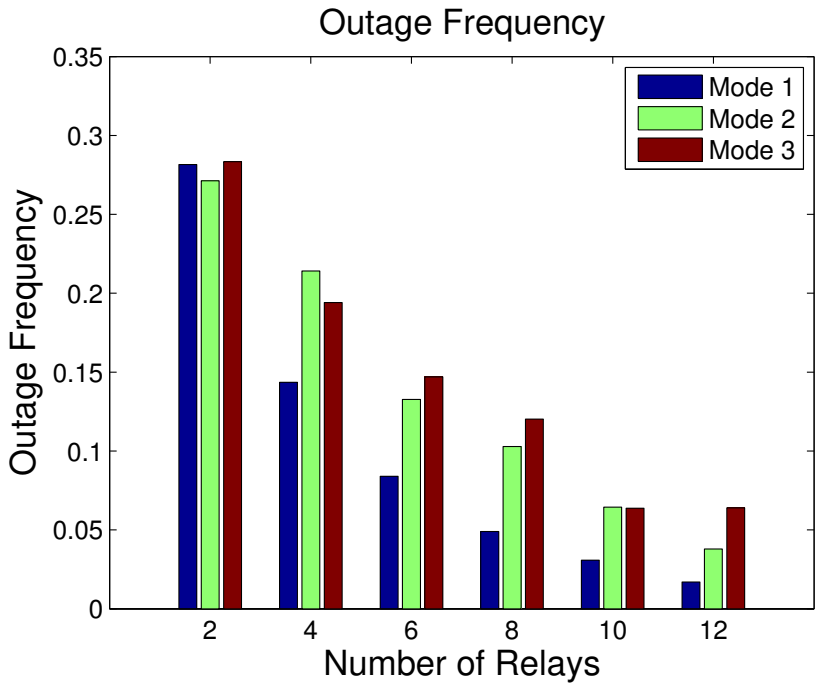

Figure 2.12: Outage Frequency of Three Modes with Different Relay Densities

outage frequency point of view. Outage frequency is defined as

$$f_{outage} = \frac{\text{Total Number of Outage Points}}{\text{Total Number of Simulation Points}}. \tag{2.25}$$

Figure 2.12 shows the result of outage frequency of the three different modes and different relay densities. From this result, we can see that Mode 1 performs better than Mode 2 and Mode 3. This is due to the randomness of the relay deployment, which works against outage prevention for this model. In some cases Mode 3 performs better than Mode 2. This occurs when most of the relays in Mode 2 are placed in deep shadow areas and are therefore ineffective.. The ideal relay deployment scheme would place relays at the edge of a deep fading area so that relays can successfully receive signals from the BS. On the average, random placement (Mode 3) is the worst choice among the three cases in our simulation.

For real-time applications, outage duration and outage frequency are both very important factors from the user experience point of view. Long outage duration and high outage frequency will lead to poor delay performance or even loss of packets. Figure 2.12 indicates that higher relay density will result in lower outage frequency. Next we investigate the outage duration experienced by the MS with different relay deployments. Outage duration performance is given in Figure 2.9, 2.10 and 2.11, which shows the cumulative distribution functions for outage durations for all three different modes. Here, we just show the distribution of outage duration from $100ms$ to $2s$ ($100ms$ is the smallest simulation time period). Under the SNR requirement given as $8dB$, it is shown that as the relay density increases, the probability of long outage duration decreases quickly. In Mode 1, with 4 relays, the probability of outage duration longer than $400ms$ is less than 10%. In Mode 2 and Mode 3, to achieve this, 6 and 8 relays are needed, respectively. For real-time video conferencing, the largest tolerable delay is around $200ms$. Our results indicate that in Mode 1 we do not need more than 6 relays to guarantee the probability of outage duration larger than $200ms$ to be less than 15%. In Mode 2 and Mode 3 more than 12 relays are needed to achieve this objective. Since we put the SNR requirement as $8dB$, which guarantees a small bit error rate (BER) of 16-QAM, the relay density needs to be high. If we reduce the SNR requirement and change the modulation, it is possible that the probability of outage duration longer than $200ms$ will become smaller or even close to 0. If there is no relay in the cell and an MS enters into a deep fading area, then due to correlated shadow fading, this outage duration will last for a long time. The longest outage duration in our simulation is $10s$ with no relay. From Figure 2.9, 2.10 and 2.11 we can observe that the probability of an outage duration greater than $2s$ is approximately 5% without relaying. Comparing the no relay case with

the 6 relays case in Mode 1, it is shown that relays efficiently reduce the lengthy outages which are caused by deep shadow fading, with the probability of outage duration greater than $2s$ reduced to less than 1%. All these results indicate that relays can mitigate the deleterious effects of correlated shadow fading efficiently.

2.6 Conclusions and Future Work

In this chapter, we investigate the correlated shadow fading problem in a single cell cellular network and shows that it could lead to correlated outage and long outage durations. A correlated outage field is presented in this chapter. To mitigate shadow fading, relays can be deployed. The performance of three different relay deployments with different relay densities are studied. Theoretical analysis and simulations of outage performance are given to compare between different relay placement scenarios. Through these simulation, we showed that uniformly spaced relays perform better than the randomly spaced, due to the randomness of relay deployment. In next several chapters, we will consider different shadow fading correlation model, which is more realistic to analyze multi-cell system. We will extend our analytic work to build a model that can predict the impact of shadow fading in a mobile environment to different parameter settings.

Chapter 3

Single-Cell System Performance Analysis under Correlated Shadow Fading

Shadow fading has been proven to be a significant contributor to channel variations in wireless communication. In most cases shadow fading is assumed to have a log-normal fading distribution to model the loss at a certain location. However, in a mobile network, it is also important to know how shadow fading is correlated both in space and in time, which can greatly affect application layer behavior and service quality. This chapter is an attempt to characterize shadow fading so as to accurately study its impact on the application layer quality of service. If the correlation is strong over time and space, shadow fading can result in a long outage. In this chapter, we assume shadow fading is exponentially correlated in space. To study correlated shadow fading and its resultant outage durations, a first-order Markov chain model is developed and validated. The Markov chain model is constructed by partitioning the entire shadow fading range

into a finite number of intervals. The state transition matrix of the Markov chain is derived from the joint probability distribution of correlated log-normal shadow fading. Based on the proposed Markov chain model, the frequency and duration of outage near the edge of a single cell is analyzed. To validate the Markov chain model, correlated Gaussian random fields are simulated to analyze the outage frequency and durations due to correlated shadow fading. Comparing the simulation results with the Markov chain model results, we can conclude that the proposed Markov chain model is an efficient way to describe the channel variations, and the user experienced outage behavior of the channel.

3.1 Background

In the past few decades, fading in wireless communication systems has been studied extensively in the literature. Fading phenomena can substantially affect the performance of a wireless communication system. In general, fading can be divided into two categories: large-scale fading and small-scale fading. A signal transmitted from source to destination will experience both large-scale and small-scale fading. Small-scale fading is caused by multipath propagation. Large-scale fading, which is also known as shadow fading, is caused by obstacles (trees, buildings, etc.) in the propagation path. Shadow fading is approximated by an independent log-normal distribution [21] in most cases. Researchers have also shown that shadow fading is spatially correlated at different positions on the propagation path [35], [36]. The spatial correlation of shadow fading is important when studying the quality of service of a mobile system since it will result in long-lasting outage durations, which will deteriorate the performance of the applications running on the network. For example, in Figure 3.1, the user is moving behind a row

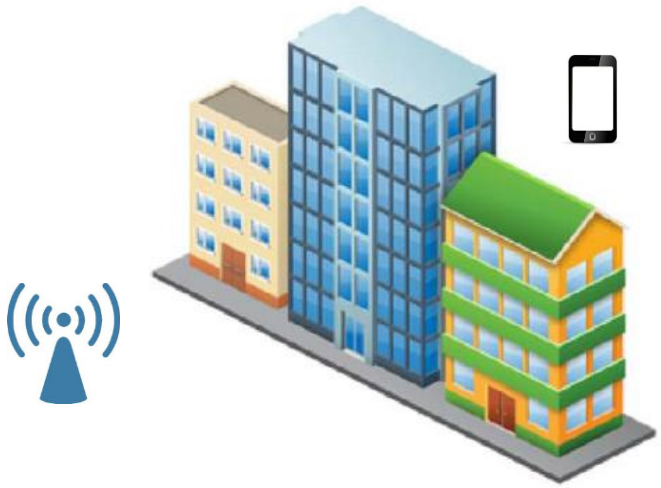

Figure 3.1: An example of building blockage.

of tall buildings which block the signals from the base station. These tall buildings result in deep shadow fading, and the shadow fading of different positions behind these buildings are closely correlated.

The spatial correlation of shadow fading has been investigated by numerous researchers. Based on empirical measurements, different autocorrelation models have been proposed for different scenarios and radio frequencies [35, 37, 38]. Szyszkowicz et al. [17] studied shadow fading correlation models and investigated the feasibility of all these models. Among all these models, the analytical model proposed by Gudmundson [35] based on empirical measurements of $900MHz$ frequency is the one which is widely used in channel estimation. This model shows that shadow fading can be modeled as a first-order autoregressive process AR(1), which indicates a spatial exponential decaying autocorrelation function. Given this model, we propose a Markov chain model that can be constructed to capture the variation of shadow fading. The Markov chain models can in turn be used to accurately model the impact of shadow fading on higher layer protocols and applications. Since the shadow fading statistically follows a log-normal distribution,

we can divide the entire range of shadow fading, which is $[-\infty, +\infty]$ into a finite number of intervals. Each interval is considered as a state of the Markov chain model. When the shadow fading falls in a particular interval, it is assigned to be in this particular state. The number of intervals (states) defines the granularity of the Markov chain model. The higher the number of states, the higher the precision in modeling the shadow fading. Correlated log-normal shadow fading has different variances with regard to different scenarios. For example, urban and suburban areas have different standard deviations based on empirical measurements. Different standard deviations of the log-normal shadow fading will result in different state transition matrices of the Markov chain model.

Outage events happen when the channel state is poor, and the received signals are not strong enough for the receiver to decode. Outage probability and the length of outage duration are important performance measurements of a wireless communication system over fading channels. Considering the applications which require low latency where buffer size is small, a long outage duration will drop the connection and lower the quality of service. To study the outage behavior of a communication system under correlated shadow fading, a well designed Markov chain model is a powerful tool. With a Markov chain model, the channel state in the next user position can be estimated from the current channel state given the current user position. Therefore, the system performance can be evaluated efficiently. Fading is a significant factor which causes dramatic channel state variations. Correlated shadow fading will result in long-lasting outage durations which is harmful to delay-sensitive real-time application and result in loss of quality of service. The Markov chain model can be used to analyze the probability distribution of outage events. The distribution and behavior of outage events will provide us the necessary information to improve wireless communication systems further.

For example, efficient cooperative communication schemes can be designed to mitigate the outage behavior.

The main focus of this chapter is how to design a first-order Markov chain model to reflect the spatial correlation of shadow fading, and the study of outage behavior of a single cell wireless communication system given correlated shadow fading. The key contributions of this chapter are summarized below.

- Constructed a Markov chain model based on correlated shadow fading.
- Analyzed the outage frequency and outage duration of a single cell wireless communication system over correlated shadow fading.

The remaining sections of this chapter are organized as follows. The channel model with spatial correlated shadow fading is described in Section 3.2. Section 3.3 shows how to construct the Markov chain model from the correlated shadow fading. Analysis of outage behavior is demonstrated in Section 3.4. Simulation to validate the Markov chain model is illustrated in Section 3.5. Section 3.6 summarizes and concludes the chapter.

3.2 Channel Model with Correlated Shadow Fading

To simplify the problem, we consider a single 4G LTE cell without any intercell interference in Figure 3.2(b). Due to the high bandwidth of OFDM systems, LTE networks are more resilient to frequency selective fading [21], therefore in this chapter small-scale fading is ignored and shadow fading becomes the most important fading factor. There is a Base Station(BS) at the center of the cell.

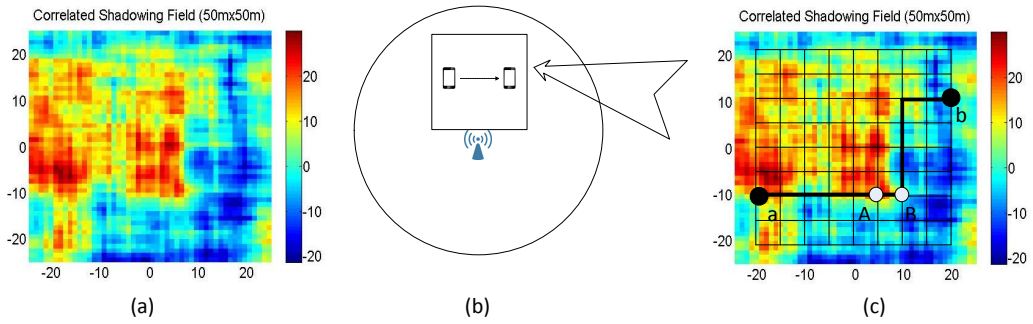

Figure 3.2: (a) A typical exponential correlated shadow fading field in a $50m \times 50m$ area. The color bar denotes the value of the shadow fading in dB. (b) A single cell model with a MS moving on a fixed trajectory. (c) A locally generated correlated shadowing field for a fixed trajectory from point a to point b.

A Mobile Station (MS) is moving on a certain trajectory within the cell. The received signal on a link $(S \rightarrow D)$ between source and destination is given by:

$$y_D = G_{SD} x_S + n_D. \tag{3.1}$$

where x_S is the signal transmitted by the source and y_D is the signal received by the destination. $n_D \sim \mathcal{CN}(0, N_0)$ is additive white Gaussian noise. G_{SD} is the channel gain from source to destination including path loss and shadow fading. SNR $\triangleq P*G_{SD}^2/N_0$, is the end-to-end received signal-to-noise ratio (SNR). The destination successfully receives the signals if no outage event happens, i.e., $\log_2(1+\text{SNR}) \geq R$, where R is the required data rate. From the definition of SNR, no outage event happens as long as $G_{SD}^2 > \beta$, where $\beta = \frac{(2^R-1)*N_0}{P}$. Therefore the channel gain from transmitter to receiver determines if an outage will occur.

Here we rewrite the channel gain in the following form: $G_{dB} = PL(d) + S$, where G_{dB} is G_{SD} in dB, PL denotes the propagation pathloss in dB, d is the distance from BS to MS and S denotes shadow fading factor. In most cases, shadow fading is modeled as an independent log-normal distribution [13] with a standard deviation derived from empirical measurements. In this model, the

probability distribution of pathloss G_{dB} is given by:

$$p(G_{dB}) = \frac{1}{\sqrt{2\pi}\sigma_{G_{dB}}} exp[-\frac{(G_{dB} - \mu_{G_{dB})^2}}{2\sigma^2_{G_{dB}}}]. \tag{3.2}$$

where $\mu_{G_{dB}}$ is the average pathloss which is equal to $PL(d)$ and $\sigma_{G_{dB}}$ denotes the standard deviation of pathloss. Since shadow fading is the only fading factor that is considered here, $\sigma_{G_{dB}}$ is determined by the standard deviation of shadow fading. This model fails to capture the spatial correlations in shadow fading. For examples, in Figure 3.2(c), shadow fading factors of two close positions A and B, which are S_A and S_B, are not independent but correlated to each other. Empirical measurements showed that shadowing has significant correlations in several realistic scenarios and the correlated shadow fading can affect system performance [14]. Among all models derived from empirical measurements for correlated shadow fading, exponentially decaying correlation [35] is widely used. In this chapter, we choose this model to do further analysis. Figure 3.2(a) is an example of exponentially correlated shadowing field which is generated from the Graziano model [14]. This figure shows a $50 \times 50m^2$ shadow fading area and illustrates that deep shadowing area is clustered and correlated (the blue area).

In Figure 3.2(c), the entire space is discretized. The MS moves on the lattice as shown. A and B are two neighbouring points. Assume the shadow fading (in dB) is $N(0, \sigma^2)$ where σ is the standard deviation, the spatial correlation between S_A and S_B will be given by

$$\rho_{A,B} = \frac{E[S_A S_B]}{\sigma^2} = e^{-\frac{d_{A,B}}{d_0}} \tag{3.3}$$

where $d_{A,B}$ is the distance between A and B, d_0 denotes the de-correlation distance

[39], which means if the distance between two points are substantially greater than d_0, the two shadow fading will be independent to each other. d_0 is determined by the environment, therefore urban and suburban areas have different de-correlation distances. An exponential correlation implies the shadow fading samples can be written as an AR(1) process as follows [40]:

$$S_B = \rho S_A + (1 - \rho) n_A \tag{3.4}$$

where n_A denotes the channel noise at A. From this we conclude that the next channel state can be determined from the current channel state and the distance MS moves.

3.3 Markov Chain Model

In this section, we will construct a Markov chain model for exponential correlated shadow fading. First of all, we will discretize the space. In Figure 3.2(c), the space was partitioned into unit square spaces of $5 \times 5m^2$ (This granularity is used to describe the Markov chain model while in the simulation we uses a finer granularity). The MS moves on the lattices from point to point, the distance between each two neighboring points are considered as a unit distance δd. We prove that shadow fading factors of any two points that can be connected by a trajectory having jointly Gaussian distribution.

Lemma 1. Exponential correlated shadow fading factors of any two points that can be connected by a trajectory have a jointly Gaussian distribution.

Proof. Suppose the two points are a and b, since there exists a trajectory connecting a and b like in Figure 3.2(c), we can assume there are n positions on this

trajectory $(t_1, t_2, \ldots, t_n)$. Then follow equation (3.4), we have the following:

$$\begin{aligned} S_b &= \rho S_{t_n} + (1-\rho) n_{t_n} \\ &= \rho(\rho S_{t_{n-1}} + (1-\rho) n_{t_{n-1}}) + (1-\rho) n_{t_n} \\ &= \ldots\ldots \\ &= \rho^n S_{t_1} + \sum_{i=1}^{n} \rho^{n-i}(1-\rho) n_{t_i} \\ &= \rho^{n+1} S_a + \rho(1-\rho) n_a + \sum_{i=1}^{n} \rho^{n-i}(1-\rho) n_{t_i} \end{aligned} \tag{3.5}$$

Let $X = \alpha S_a + \beta S_b$, from equation 3.5, the following can be derived:

$$X = \alpha S_a + \beta(\rho^{n+1} S_a + \rho(1-\rho) n_a + \sum_{i=1}^{n} \rho^{n-i}(1-\rho) n_{t_i}) \tag{3.6}$$

Since S_a, n_{t_i} and n_a are all independent and Gaussian random variables, we conclude that X is also Gaussian, which implies that S_a and S_b are jointly Gaussian. □

Given the above conclusion, a Markov chain model can be constructed as follows:

- Divide the entire shadow fading range $[-\infty, +\infty]$ into a finite number of intervals $\{[-\infty, S_0], [S_0, S_1], \ldots, [S_N, +\infty]\}$. Each interval represents a state of the Markov chain model.
- Derive the state transition matrix of the Markov chain model from the probability distribution of the correlated shadow fading.
- Derive the steady-state probability from the state transition matrix of the Markov chain model.

To derive the state transition matrix of the Markov chain model, we first investigate the probability density function of the correlated shadow fading. Since we have discretized the entire space into unit distances, here the state transition probability from point A to point B will be defined and used to calculate the state transition matrix of the Markov chain. Since S_A and S_B are jointly Gaussian with a correlated coefficient ρ_0, according to [41], we have

$$\begin{aligned} f_{S_A|S_B=s_B}(s_A) &= \frac{f_{S_A,S_B}(s_A,s_B)}{f_{S_B}(s_B)} \\ &= \frac{1}{\sigma_A\sqrt{2\pi(1-\rho_0^2)}}\exp\{-\frac{(s_A-(\mu_A+\sigma_A\rho_0(s_B-\mu_B)/\sigma_B))}{2\sigma_A^2(1-\rho_0^2)}\} \end{aligned} \tag{3.7}$$

where μ_A and μ_B are expectations of log-normal shadow fading S_A and S_B, which is typically set to 0, while σ_A and σ_B are standard deviations, which are assumed to be equal to σ_0. Based on these assumptions, we can rewrite the equation as follows:

$$f_{S_A|S_B=s_B}(s_A) = \frac{1}{\sigma_0\sqrt{2\pi(1-\rho_0^2)}}\exp\{-\frac{s_A-\rho_0 s_B}{2\sigma_0^2(1-\rho_0^2)}\} \tag{3.8}$$

Assume there are N states of the Markov chain model $ST_1, ST_2, \cdots, ST_N$ where ST_i corresponds to the interval $(S_{i-1}, S_i]$. Then we have the state transition probability as follows:

$$\begin{aligned} P_{i,j} &= P(S_A \in ST_j | S_B \in ST_i) \\ &= \frac{P(S_A \in ST_j, S_B \in ST_i)}{P(S_B \in ST_i)} \\ &= \frac{\int_{S_{i-1}}^{S_i}(\int_{S_{j-1}}^{S_j} f_{(S_A|S_B=s_B}(s_A)ds_A)f(s_B)ds_B}{\int_{S_{i-1}}^{S_i} f(s_B)ds_B} \end{aligned} \tag{3.9}$$

From equation (3.9), the state transition matrix of the Markov chain can be derived. The steady-state transition matrix can be determined by P.

3.4 Analysis of Outage Behavior

In this section we analyze the outage behavior of the communication system using the Markov chain model of correlated shadow fading. The outage duration of a system is a significant factor influencing system performance. Given a fixed mobile trajectory, the Markov chain model described in Section 3.3 provides an efficient way to study the outage events. In Figure 3.2(c), a fixed trajectory is given from point a to b through several intermediate points. Considering two consecutive points A and B, we have $G_A = PL_A(d_A)+S_A$ and $G_B = PL_B(d_B)+S_B$ in dB. The probability that A and B are both in an outage area can be written as:

$$\begin{aligned} &P(G_A < \gamma, G_B < \gamma) \\ &= P(S_A < \gamma - PL_A(d_A), S_B < \gamma - PL_B(d_B)) \end{aligned} \tag{3.10}$$

If $S_A < \gamma - PL_A(d_A) \in ST_i$ and $S_B < \gamma - PL_B(d_B) \in ST_j$, we can infer that, to avoid outage, the lower bound of the shadow fading factor S_A is in state ST_i and for S_B is in state ST_j. State ST_i and ST_j are called lower bound states. Based on this approximation, the above probability can be written as:

$$P(G_A < \gamma, G_B < \gamma) = \sum_{m=0}^{i} \sum_{n=0}^{j} P(ST_m) \bullet P(ST_m, ST_n) \tag{3.11}$$

where $P(ST_m)$ is the probability that S_A is in the range of ST_m which can be calculated from the Gaussian distribution. $P(ST_m, ST_n)$ can be found from the state transition matrix. Following this, the probability of an outage duration of

$$P = \begin{bmatrix} P1 \\ P2 \\ P3 \\ P4 \\ P5 \\ P6 \\ P7 \\ P8 \end{bmatrix} \tag{3.13}$$

length $l > L$ can be derived in below:

$$\begin{aligned} &P(G_1 < \gamma, \ldots, G_L < \gamma) = \\ &\sum_{m_1=0}^{M_1} \cdots \sum_{m_L=0}^{M_L} P(ST_{m_1}) \bullet P(ST_{m_1}, ST_{m_2}) \\ &\bullet \ldots \bullet P(ST_{m_{L-1}}, ST_{m_L}) \end{aligned} \tag{3.12}$$

where M_i, $i \in \{1, \ldots, L\}$ are corresponding lower bound states of each position on the trajectory.

$$
\begin{aligned}
P1 &= \begin{bmatrix} 0.5580 & 0.3627 & 0.0757 & 0.0036 & 3.5243\times10^{-5} & 0 & 0 & 0 \end{bmatrix} \\
P2 &= \begin{bmatrix} 0.1587 & 0.4404 & 0.3359 & 0.0624 & 0.0026 & 2.3466\times10^{-5} & 0 & 0 \end{bmatrix} \\
P3 &= \begin{bmatrix} 0.0184 & 0.1788 & 0.4546 & 0.2980 & 0.0484 & 0.0018 & 1.4485\times10^{-5} & 0 \end{bmatrix} \\
P4 &= \begin{bmatrix} 0.0007 & 0.0258 & 0.2165 & 0.4624 & 0.2573 & 0.0361 & 0.0012 & 8.4341\times10^{-6} \end{bmatrix} \\
P5 &= \begin{bmatrix} 8.4341\times10^{-6} & 0.0012 & 0.0361 & 0.2573 & 0.4624 & 0.2165 & 0.0258 & 0.0007 \end{bmatrix} \\
P6 &= \begin{bmatrix} 0 & 1.4485\times10^{-5} & 0.0018 & 0.0484 & 0.2980 & 0.4546 & 0.1788 & 0.0184 \end{bmatrix} \\
P7 &= \begin{bmatrix} 0 & 0 & 2.3466\times10^{-5} & 0.0026 & 0.0623 & 0.3359 & 0.4404 & 0.1587 \end{bmatrix} \\
P8 &= \begin{bmatrix} 0 & 0 & 0 & 3.5243\times10^{-5} & 0.0036 & 0.0757 & 0.3627 & 0.5580 \end{bmatrix}
\end{aligned}
\tag{3.14}
$$

In this section, we employ Monte-Carlo simulation to validate our Markov chain model. To start the simulation, a large number of correlated shadowing fields are generated. As shown in Figure 3.2(b) and (c), instead of generating shadowing fields for the entire cell, we pick up a MS trajectory and generated shadowing fields that covers that trajectory. In this chapter, we choose the urban environment as the case to study. In this case, the shadow fading and Markov chain parameters are set as in Table 3.1. The standard deviation of shadow fading is chosen to be $8dB$ following [17]. The number of states of the Markov chain is set to be $3 * \sigma_0/n * 2 + 2$, where $n = 1, 3, 8$ is the size of each range (state) in dB except the two above $3\sigma_0$. n in this case represents different granularities in the area of $[-3\sigma_0, 3\sigma_0]$. The state transition matrices are calculated with regard to

Table 3.1: Simulation Configuration Parameters

Okumura-Hata Model	BS Height: $100m$ MS Height: $1m$
	De-Correlation Distance d_0: $20m$ Standard Deviation σ_0: $8dB$
Correlated Shadow Fading Markov Chain Model	Number of States: 50, 18, 8 $(3 * \sigma_0/n * 2 + 2,\ n = 1, 3, 8)$
MS Trajectory	Unit Distance δd: $1m$
Shadowing Field	$50 \times 50m^2$
Radio Frequency	$f : 1024MHz$
BS Transmission Power	$P : 30dbm$
SNR Requirement	$10dB$

each n. For example, when $n = 8$, the states of the Markov chain model are:

$$\begin{aligned}&[(-\infty, -24], (-24, -16], (-16, -8], (-8, 0],\\ &[0, 8], [8, 16), [16, 24), [24, +\infty)]\end{aligned} \tag{3.15}$$

and the state transition matrix is given in (3.13 and 3.14).

3.5 Simulation Results

To validate our Markov chain models, the probability distributions of outage durations corresponding to MS trajectories of length $l > 1m$ up to $l > 9m$ are studied given different number of states. Since there is a trade-off between the number of states and the complexity of the simulation computation, the simulated results also provide us information about the proper granularity of the Markov chain model to most accurately approximate the real channel. The simulation also confirms that correlated shadow fading indeed can cause long-lasting outage durations. In our simulation, the MS moves on a straight track which is around

$900m$ away from the BS. Let l denote the outage duration in meters, Figure 3.3 shows the probability of $l > L$. Comparing the two cases: with and without correlation, we can conclude that correlated shadow fading can result in severe long-lasting outage durations. Take $L = 5$ for example, the correlated case gives $P(l > L) = 12\%$, while in the non-correlated case the probability is around 0%. This illustrates the correlation between shadow fading cannot be neglected in mobility models. The MS speed is approximately the same as pedestrian speed which is $1m/s$ (Since the edge length of the lattice is $1m$, the MS moves one grid (unit distance) every second). Assuming this, the user will experience an outage of more than 9 seconds with a probability of 7%.

To find out the proper number of states of the Markov chain model, three different Markov chain models with different number of states are tested. Basically we divide the $[-3\sigma_0, 3\sigma_0]$ area with different granularity, which is represented by $n = 1, 3, 8$. When $n = 1$, the interval ST_i except $(-\infty, S_0]$ and $[S_N, +\infty)$ is $1dB$. The results showed in Figure 3.3 indicates that when $n = 1$, the curve is close to the correlation curve, which means that the Markov chain model becomes a good approximation of the channel to study the outage behavior of the system. Generally, more Markov states lead to more precise models. When the interval $[S_i, S_j]$ becomes relatively large with regarding σ_0, the Markov chain model will fail to be a useful tool to study the outage behavior of the system. For example, in Figure 3.3, when $n = 8$, $P(l > 1)$ is almost twice the correct $P(l > 1)$. The prediction of the outage behavior of the system is not precise and useful anymore.

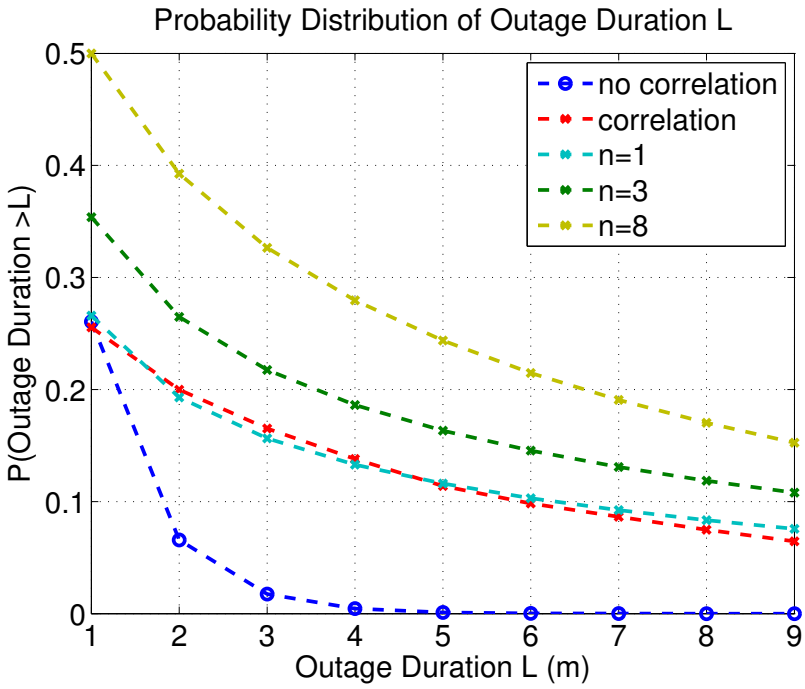

Figure 3.3: Probabilities of outage duration greater than L.

3.6 Conclusions

In this chapter we investigated how shadow fading at different positions in a cellular network is correlated. In an environment where the correlation is high, shadow fading will result in long-lasting outage durations which can lead to a significant deterioration in system performance. To model spatially correlated shadow fading we divided the entire range of shadow fading into a finite number of intervals. A Markov chain model is then constructed, where each interval becomes a state of the Markov chain model. This model can be used to analyze the outage behavior at the application layer. We demonstrated that a well designed Markov chain model with an appropriate number of states corresponding to the standard deviation of the shadow fading is indeed a powerful tool to study system performance. For a single-cell system, this Markov chain model is able to analyze the system performance because there only exist autocorrelation in this scenario.

In next chapter, we will investigate the system performance of a multi-cell communication system. This model will not be capable to describe the scenario there. We will run simulations to show the system performance of a multi-cell system under exponentially correlated shadow fading.

Chapter 4

Multi-Cell System Performance Analysis under Correlated Shadow Fading

In a cellular network, connections between the Base Station (BS) and Mobile Users (MUs) may fail when the channel is in deep fade. Shadow fading is large-scale fading which can cause significant received power loss for a wide area. Correlated shadow fading will result in correlated long outage durations. Power outage will lead to connection loss and/or packet loss which is harmful to MUs, especially to those who are using real-time applications such as video conferencing. Intuitively, increasing BS density is considered to be an efficient way to reduce outage and provide better Quality of Service (QoS) support for delay sensitive applications in noise-limited regime. This chapter is an extension of Chapter 3, which focuses on a study of the performance of a multi-cell communication system under correlated shadow fading. We consider the downlink direction in a multi-cell communication system. To investigate the outage probability given

correlated shadow fading and different BS densities, two system layouts, Grid model and Random model, are studied. First, we compare the outage probability with same correlated shadow fading with regard to the two different system layout. Grid layout performs better than Random layout. Secondly, we compare the outage probability with independent shadow fading and with the correlated shadow fading for Random model. The received signal-to-interference-plus-noise ratio (SINR) is calculated by assuming independently Gaussian and jointly Gaussian shadow fading at the MU. Thirdly, we focused on Random model which is more realistic and compared the outage duration under two circumstances: independent shadow fading and correlated shadow fading. Simulation results show that the outage durations with correlated shadow fading are longer than that of the independent shadow fading. At last, we showed that increasing BS density can reduce the effect of correlated shadow fading and improve the system performance in terms of outage probability and outage duration.

4.1 Background

In a cellular communication system, the connection between the BS and a MU may be dropped when the user enters a deeply shadowed area. Fading phenomena can substantially affect the performance of a wireless communication system. In general, fading can be divided into two categories: large-scale fading and small-scale fading. A signal transmitted from source to destination will experience both large-scale and small-scale fading. Small-scale fading is caused by multipath propagation. Large-scale fading, which is also known as shadow fading, is caused by obstacles (trees, buildings, etc.) in the propagation path. In most cases, shadow fading is assumed to be temporally and spatially independent [21]. Researchers

have also shown that shadow fading is spatially correlated at different positions on the propagation path [35], [36]. In [22] and [23], the effects of correlated shadowing in connectivity is demonstrated, which indicates that reliable connectivity will be much more difficult to maintain than indicated by independent shadow fading models. The spatial correlation of shadow fading is important when studying the quality of service of a mobile system since it will result in long-lasting outage durations, which will deteriorate the performance of the applications running on the network. The focus of this chapter is to study channel variations and system performance due to correlated shadow fading in a multi-cell communication system and provide a solution to reduce the frequency and duration of dropped connections and improve system performance by increasing BS density.

There have been a lot of studies on the outage probability of cellular communication systems [42–44]. The author of [45] analyzed the outage probability and coverage area under different independent identical distributed (i.i.d.) shadow fading distributions: Log-normal distribution, Weibull distribution and Gamma distribution. In contrast, there is much less work on the outage probability and outage duration given correlated shadow fading. The system performance of multi-cell system given correlated shadow fading is still an open problem. In [46] and [47] we studied the outage probability and outage duration of a single cell communication system under exponentially correlated shadow fading and Distance-Angle correlated shadow fading. [46] we showed that for a single cell model, exponentially correlated shadow fading can be modeled as a Markov Chain Model. Highly correlated shadow fading will result in long-lasting outage durations. In [47], single cell given distance-angle correlated shadow fading system is studied. The correlated shadow fading also lead to correlated outage and long outage durations in a single cell model. In this case, we provide a solution to overcome the correlated

shadow fading: relay cooperative communication. Chapter 2 and Chapter 3 are limited to single-cell model. In this chapter, we are going to extend the study of correlated shadow fading impact to a multi-cell communication system, and provide a solution to overcome the long-lasting outage duration.

For multiple-cell system, in [48], the author develop new general models for the multi-cell signal-to-interference-plus-noise ratio (SINR) using stochastic geometry. The cellular networks is modeled by placing the BSs at locations as a homogeneous Poisson Point Process. The author concluded that under general fading, increasing the number of BSs does not affect the coverage probability (so is the outage probability) while the MU is connected to the nearest BS. The paper also did comparison between grid model and the random PPP model and concluded that a regular grid provided the upper bound of the coverage probability while the PPP provided the lower bound. The author also considered the effect on independent log-normal interference and concludes that the increasing log-normal interference increased the coverage probability which seems counter-intuitive. In this paper, the author didn't consider the scenarios with correlated log-normal interference. Only the coverage probability is studied, analysis of outage duration is not analyzed.

A comparative study of random and grid topology of small cell network deployment was given in [49]. In this paper, spatial outage probability and spatial average throughput versus the number of access points of the two different network deployment is studied. But this paper considered independent log-normal interference instead of correlated log-normal fading. Approximate outage probability and capacity for $\kappa - \mu$ shadow fading is studied in [50]. $\kappa - \mu$ shadow fading includes one-side Gaussian, the Rayleigh, the Nakagami-m, the Rician. As we mentioned before, the imperial measurements didn't exhibit such complicated

features of shadow fading. So comparing with correlation, those complex features are not of main focus.

As we have mentioned in previous chapters, in most cases shadow fading is modeled as an independent log-normal distribution. But this model fails to capture the spatial correlations in shadow fading. This chapter contains three major sections: first part describes the correlated shadow fading model that was used and the resulting correlated outage field; second part studies the outage probability given Grid layout and Random layout; third part investigates the outage probability and outage duration of the system given different BS densities, different correlation parameters and different connection strategies. The key contributions of this chapter are summarized below.

- Correlated outage fields are given to analyze the relationship between correlated shadow fading and correlated outage events.
- Investigate outage probability analysis of both Grid layout and Random layout.
- Show how increasing BS densities help mitigate correlated shadow fading in Random layout in terms of outage probability (coverage probability) and outage durations.
- Analyze the relation between the tunable parameter of the correlated shadow fading model and the outage probabilities.
- Compare the system performance of different MU-BS connection strategies: MU connecting to the nearest BS and MU connecting to the BS providing strongest signal.

The chapter is organized as follows: Section 4.2 presents the correlated shadow fading model that is used in this paper and the resultant correlated outage field. Section 4.3 presents the system model with two different BS deployment schemas and investigates the outage probability given different BS layout. Section **??** gives theoretical analysis of outage probability given correlated shadow fading. Section **??** presents the simulation setup and analyzes the simulation results of different BS deployments and densities. Section **??** summerizes the chapter and proposes future work directions.

4.2 Correlated Shadow Fading

As stated in the background, empirical measurements show that there exist different patterns of correlations between the shadowing. The independent log-normal shadow fading model, while very useful for static MS performance analysis, cannot reflect the correlation of shadow fading between different locations. In this section, we will give a brief introduction of shadow fading models, including the model used in this chapter. There is no single mathematical model which captures all different categories of correlation [17]. In Chapter 2, a distance-angle correlation model is used and in Chapter 3 an exponential correlation model is used. The correlation matrix of angle-distance model is given below:

$$\mathbf{K}_{N\times N} = [\sigma_s(\vec{r_i})\sigma_s(\vec{r_j})h(\vec{r_i}\vec{r_j})], \tag{4.1}$$

where N paths interfere with path $\vec{r_i}$ and $\mathbf{E}\{S_i^2|\vec{r_i}\} = \sigma_s^2(\vec{r_i})$. This model assumes that in the correlation matrix, h is separable with respect to the angle of arrival

$$\theta = |\angle\vec{r_i} - \angle\vec{r_j}| \in [0^\circ, 180^\circ], \tag{4.2}$$

and the arrival distance ratio

$$R = |10\log_{10} r_i/r_j| = \frac{10}{\ln 10}|\ln r_i - \ln r_j|, \tag{4.3}$$

$$h(\vec{r_i}, \vec{r_j}) = max\{1 - \theta/\theta_0, 0\} \cdot max\{1 - R/R_0, 0\}. \tag{4.4}$$

The correlation coefficients is a piece-wise linear function of the angle of arrival and the arrival distance ratio. Due to this feature, when cell size decreases (BS density increases), the correlation between two points also decreases. This violate the physical characteristic of shadow fading. The size of obstacle which causes the shadow fading does not change when the cell size changes, therefore the correlation between two different position should not change when cell size changes. As stated above, the angle-distance model is not suitable for analyzing mulit-cell system performance. In this chapter, we use the exponentially correlated shadow fading model [19] the same as in Chapter 3. In [19], the author states that correlation in shadowing is indispensable for the analysis of interference of large networks. An exponentially correlated shadowing field S with shadow fading factor s_i for each position p_i has a correlation matrix as below:

$$\mathbf{K}_{N\times N} = [\sigma_s(p_i)\sigma_s(p_j)\rho(i,j)], \tag{4.5}$$

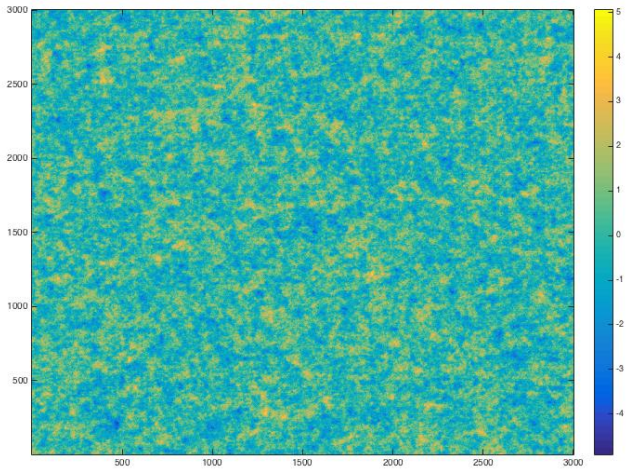

Figure 4.1: Exponentially correlated shadowing field with $d_0 = 20m$ (the color of the area refers to the normalized standard deviation which is $S_i/\sigma_s(i)$)

where N is the length of the shadowing field. Suppose A and B are two neighbouring points, the shadow fading (in dB) is $N(0, \sigma^2)$ where σ is the standard deviation. The spatial correlation between s_A and s_B will be given by

$$\rho_{A,B} = \frac{E[s_A s_B]}{\sigma^2} = e^{-\frac{d_{A,B}}{d_0}} \tag{4.6}$$

Following the shadowing field generation algorithm, we generate shadowing fields with different values of de-correlation distances. A sample shadowing field is shown in Figure 4.1.

Let $\varphi = \{1, 2, \ldots, N\}$ denotes the set of all Base Stations, then the received signal from Base Station j to the destination user D is given by:

$$y_{i \to D} = G_{i \to D} x_i + n_D. \tag{4.7}$$

where x_i is the signal transmitted by the source Base Station and $y_{i \to D}$ is the signal

received by the destination. $n_D \sim \mathcal{CN}(0, N_0)$ is additive white Gaussian noise. $G_{i\to D}$ is the channel gain from source Base Station to destination including path loss and shadow fading. The end-to-end received signal-to-interference-plus-noise ratio SINR is given as follows:

$$\text{SINR} \triangleq \frac{P_i * G_{i\to D}^2}{N_0 + \sum_{j\in\varphi/i} P_j * G_{j\to D}^2}, \tag{4.8}$$

where P_i is the transmitted power of Base Station i. The destination successfully receives the signals if no outage event happens, i.e., $\log_2(1+\text{SINR}) \geq R$, where R is the required data rate. From the definition of SINR, no outage event happens as long as $\text{SINR} > \gamma$, where $\gamma = 2^R - 1$.

Given a correlated shadowing field, the outage events at different locations are also correlated. Without considering other small-scale fading, the channel gain at different locations has a spatial correlation. Given a proper threshold γ, an outage area is defined as channel gain less than γ. Based on the aforementioned correlated shadow fading model and Random system model, a correlated outage filed can be generated as in Figure 4.2. On the left, a correlated outage field with independent log-normal shadow fading is shown while the correlated outage field with correlated shadow fading is given on the right. The black color indicates outage areas. Outage area with i.i.d. shadow fading are nonconsecutive dots while with correlated fading are connected areas. This demonstrates correlated outage areas come with correlated shadow fading.

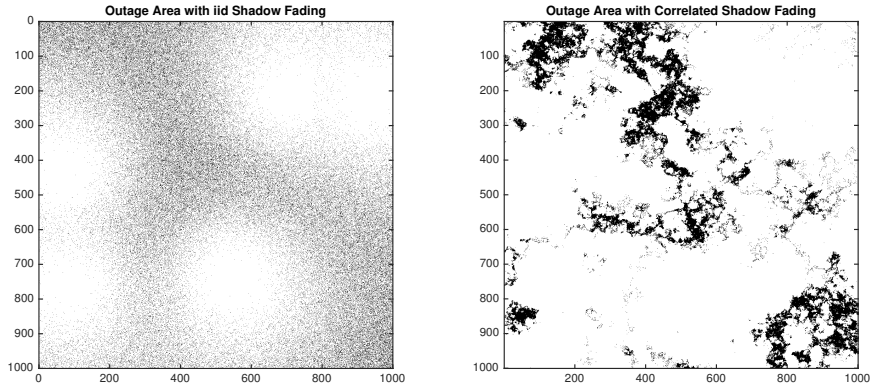

Figure 4.2: Correlated Outage Fields with γ (Dark areas are outage areas while white areas are non-outage areas)

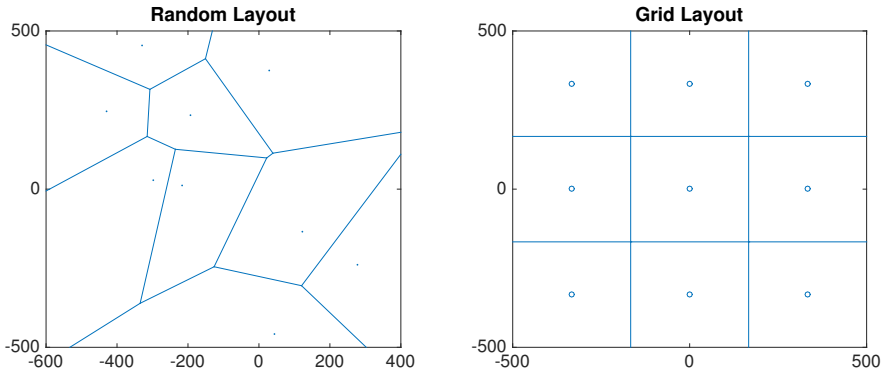

Figure 4.3: Random Layout and Grid Layout with $\lambda = 9$.

4.3 System Model

In this paper, we considered two system models with two different BS deployment scheme: Grid model and Random model.

- Grid Model: λ BSs are placed on a regular grid deterministically.
- Random Model: λ BSs are placed randomly in a fixed area.

Left figure of Fig 4.3 is an example of the traditional grid model, where cells are in regular square shape with same size. For the Random model showed in Fig 4.3 right subfigure, cells are not guaranteed to be the same shape and same size.

Nearest distances between different cells are in a large variation.

4.4 Outage Probability Analysis

Let $\varphi = \{1, 2, \ldots, N\}$ denotes the set of all Base Stations, then the received signal from Base Station j to the destination user D is given by:

$$y_{i\to D} = G_{i\to D} x_i + n_D. \tag{4.9}$$

where x_i is the signal transmitted by the source Base Station and $y_{i\to D}$ is the signal received by the destination. $n_D \sim \mathcal{CN}(0, N_0)$ is additive white Gaussian noise. $G_{i\to D}$ is the channel gain from source Base Station to destination including path loss and shadow fading. The end-to-end received signal-to-interference-plus-noise ratio SINR is given as follows:

$$\text{SINR} \triangleq \frac{P_i * G_{i\to D}^2}{N_0 + \sum_{j\in\varphi/i} P_j * G_{j\to D}^2}, \tag{4.10}$$

where P_i is the transmitted power of Base Station i. The destination successfully receives the signals if no outage event happens, i.e., $\log_2(1+\text{SINR}) \geq R$, where R is the required data rate. From the definition of SINR, no outage event happens as long as SINR $> \gamma$, where $\gamma = 2^R - 1$.

Given a correlated shadowing field, the outage events at different locations are also correlated. Without considering other small-scale fading, the channel gain at different locations has a spatial correlation. Given a proper threshold γ, an outage area is defined as channel gain less than γ.

For a particular MU, outage happens when its received SINR is less than a threshold to decode the received signal. In our scenario, the probability that the

receiver cannot decode signals received from its serving Base Station is defined as:

$$P(out_i) = P[\text{SINR}_{i\to D} < \gamma], \tag{4.11}$$

We investigate two connection strategies: MU connect to the nearest BS and MU connect to the BS provides strongest signal. If we assume that the user is served by the nearest Base Station, then the outage probability will be $P_{out} = P_{out_i}$ where i is the index of the nearest Base Station. Otherwise, the indices of all Base Stations which are able to provide successfully connection to the Mobile User form a set $\mathcal{R}_n$. Under the assumption that an MS always connecting to the Base Station which provides the best received signal, the outage event happens if no Base Station can provide big enough SINR to the receiver, which means $\mathcal{R}_0 = \phi$. Based on this assumption we have:

$$P_{out} = \max_{i=1,\cdots,N} P[\text{SINR}_{i\to D} < \gamma]. \tag{4.12}$$

The probability density function (pdf) of shadow fading S given L correlated fading branches is

$$\begin{aligned} f_{\mathbf{S}}(\mathbf{s}) =& \frac{\lambda^L}{\sqrt{2\pi}|\mathbf{K}_{L\times L}|^{1/2}\prod_{i=1}^{L} s_i} \\ & \cdot \exp(-\frac{1}{2}(10\log_{10}\mathbf{s} - \boldsymbol{\mu})^T \mathbf{K}_{L\times L}^{-1}(10\log_{10}\mathbf{s} - \boldsymbol{\mu})), \end{aligned} \tag{4.13}$$

where $\lambda = 10/\ln 10$ and $\boldsymbol{\mu}$ is the average shadow fading which is normally 0. $\mathbf{K}_{L\times L}$ is the correlation matrix which is defined in (4.5). Let $\theta_i = \frac{10\log_{10} s_i - \mu_i}{\sqrt{2}\sigma_i}$, and doing a change of variables gives us the pdf of $\boldsymbol{\Theta}$ as follows:

$$f_{\boldsymbol{\Theta}}(\boldsymbol{\theta}) = \frac{1}{\pi^{(L/2)}|\boldsymbol{\Sigma}|^{1/2}} \exp(-\boldsymbol{\Theta}^T\boldsymbol{\Sigma}^{-1}\boldsymbol{\Theta}), \tag{4.14}$$

$$g(PL_iS_i-\gamma\sum_{j\in\varphi/i}PL_jS_j)=\begin{cases}1, & \text{when } PL_iS_i-\gamma\sum_{j\in\varphi/i}PL_jS_j<\frac{\gamma N_0}{P}\\ 0, & \text{when } PL_iS_i-\gamma\sum_{j\in\varphi/i}PL_jS_j>\frac{\gamma N_0}{P}\end{cases}. \quad (4.18)$$

---

where $\mathbf{\Sigma}$ is the correlation coefficient matrix which is

$$\begin{bmatrix} 1 & h_{1,2} & \cdots & h_{1,L} \\ \vdots & \ddots & \ddots & \vdots \\ h_{L,1} & h_{L,2} & \cdots & 1 \end{bmatrix}. \quad (4.15)$$

Since $\text{SINR}_{i\to D}=PL_{i\to D}+S_i-N_0-\sum_{j\in\varphi/i}(PL_{j\to D}+S_j)$ in dB, $\text{SINR}_{i\to D}<\gamma$ means

$$S_i-\sum_{j\in\varphi/i}S_j<\gamma-PL_{i\to D}+\sum_{j\in\varphi/i}PL_{j\to D}+N_0, \quad (4.16)$$

Then with the assumption that users are served by the nearest Base Station or the best channel Base Station, the outage probability can be written as:

$$P_{out}=\underbrace{\int_{-\infty}^{+\infty}\cdots\int_{-\infty}^{+\infty}}_{i=1,\cdots,N}g(PL_iS_i-\gamma\sum_{j\in\varphi/i}PL_jS_j)f(\mathbf{s})d\mathbf{s}. \quad (4.17)$$

where $\mathbf{s}$ is the correlated shadow fading experienced by all Base Stations, $g(PL_iS_i-\gamma\sum_{j\in\varphi/i}PL_jS_j)$ is a step function defined in (4.18).

4.5 Simulation Results

In this section, we will present simulation setup and results. First, we run simulations to compare the outage probability of the two different network topology: Grid Layout and Random Layout. Secondly, SINR distribution and outage

Table 4.1: Simulation Configuration Parameters

Study Area	$1000m \times 1000m$
BS Densities	$3, 10,$
Pathloss Exponent	4
BS Transmission Power	$P : 40dbm$
SNR Requirement	$-5dB$
De-Correlation Distance	$20m, 200m$

probability of Random Layout given different BS densities are investigated. Two scenarios are considered: MU connecting to the nearest BS and MU connecting to the BS providing strongest signal. At the end, the outage duration distribution are simulated and discussed given different BS densities. The values of parameters that are used in the simulation are shown in Table 4.1.

Figure 4.4 shows the Cumulative Distribution Function (CDF) of SINR when MU connecting to the nearest BS. The de-correlation distance of the correlated shadow fading is $20m$. The figure suggests that Grid Layout outperforms the Random Layout, which is consistent with findings in [48]. Figure 4.5 shows the outage probability with SINR threshold $-5dB$. The outage probability of Grid Layout (blue) is lower than the Random Layout (yellow). In next section, we will focus on the Random Layout which is realistic than Grid Layout.

For Random Layout, SINR distribution and outage probability of different BS densities are investigated for both nearest BS connection and best channel BS connection.

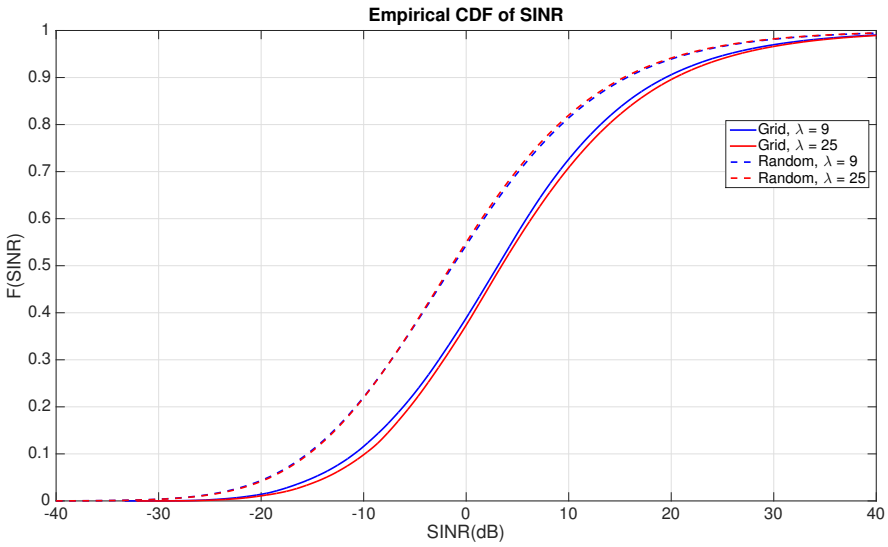

Figure 4.4: CDF of SINR given Grid Layout and Random Layout (De-Correlation Distance: $20m$)

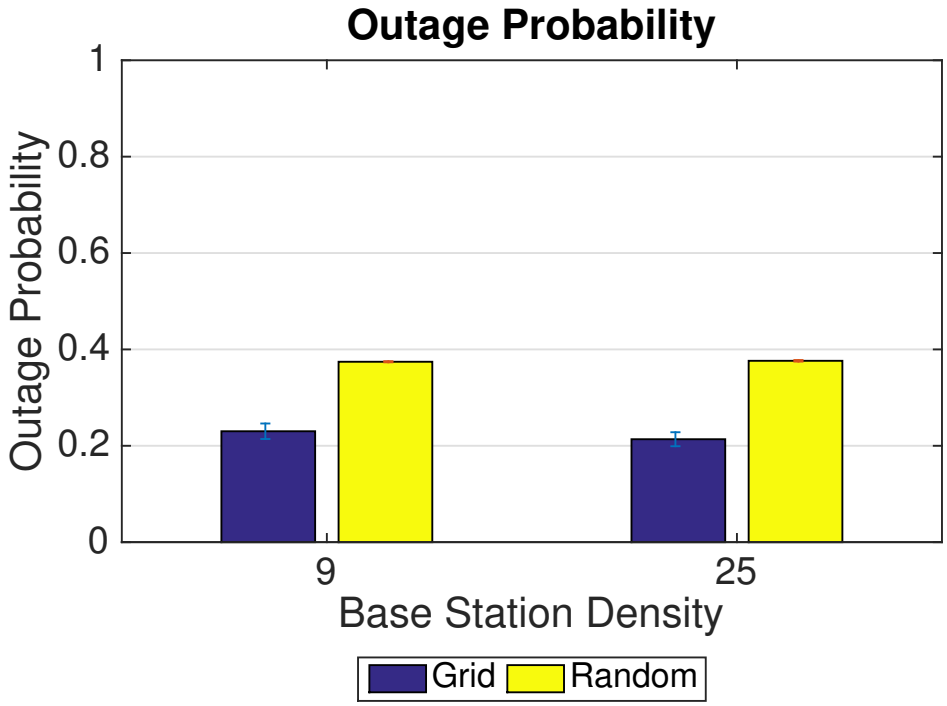

Figure 4.5: Outage Probability given Grid Layout and Random Layout (De-Correlation Distance: $20m$)

Chapter 5

Transport Layer Protocols for 5G

The rapid increase of use of smartphones generate dramatical demand increase for capacity in mobile broadband communications every year. The wireless carriers and researchers are motivated to explore the underutilized millimeter wave (mmWave) frequency spectrum for next generation (Fifth Generation) broadband cellular communication networks. Fifth generation (5G) mmWave communication system will provide high speed, high capacity wireless communication networks to users. Meanwhile, 5G mmWave channel is sensitive to obstructions, which result in high fluctuations. Legacy transmission control protocols (TCP) might not work properly with the new channel. Therefore, we first investigate the performance of legacy TCP on 5G mmWave channel. The result illustrates that 5G mmWave channel requires a fast congestion detection scheme and an aggressive recovery scheme. In this chapter, we focus on fast congestion detection scheme and present a new end-to-end TCP congestion detection scheme for high speed network: Virtual Explicit Congestion Notification (Virtual ECN), which makes the design of fast reacting congestion control protocol to be promising.

5.1 Introduction

mmWave channel provides tremendous amount of capacity and relatively low delay while it suffers high propagation loss and sensitivity to blockage. Simulations and measurements showed that the capacity gain is significant comparing with current cellular systems in [51, 52]. The last hop wireless channel capacity is not a bottleneck problem anymore. Meanwhile, mmWave channels are prone to variations due to the blockage from walls, trees, or even human body [53–55]. This feature brings frequent capacity variations to the channel. Typically, the channel switches periodically between Line-of-Sight (LOS) and Non-Line-of-Sight (NLOS). The upper layer channel provided by mmWave communication network is not standardized yet. But generally, there is a consensus that 5G mmWave channel will provide high capacity and low latency with frequent capacity fluctuation. For 5G mmWave wireless communication network, the legacy TCP congestion control might not work well due to the slow congestion detection and conservative loss recovery. Our investigation on legacy TCP with mimic 5G mmWave channel confirms this. Therefore designing a new TCP congestion control scheme without involving any intermediate network device is necessary. In this chapter, we are addressing the initial step to design such a scheme: design an end-to-end fast data driven congestion detection algorithm.

In recent years, several promising TCP congestion control protocols are developed: BIC TCP [56], CUBIC TCP [57], Compound TCP [58], etc. Most of these TCP congestion control schemes rely on three duplicated ACKs or Time Out to detect the congestion and packet loss. This means TCP needs to wait for at least 3 ACKs or a time out timer before entering into recovery mode or slow start mode. The slow congestion detection will deteriorate the network performance for

a high capacity, low latency mmWave channel with frequent capacity variation. First, for high capacity link, during this time interval, more congestion and packet loss might occur and cause high payoff to recover from the loss. Secondly, for a frequent capacity variation network whose link capacity is fluctuate significantly, the slow congestion detection scheme might provide out of date information of the congestion status, which makes the TCP congestion control protocol extremely conservative.

This chapter is organized as follows: Section 5.2 explains the related work on TCP congestion control and mmWave channel. Motivations to design this scheme is demonstrated in this section. In section 5.3, we investigate the legacy TCP congestion control performance on mimic 5G channel, for both NewReno and Cubic. Section 5.4 demonstrates our design of the fast end-to-end congestion detection scheme in detail including network simulation setup, data process and congestion prediction. Section 5.5 summarize the chapter and propose future work which can be accomplished based on this scheme.

5.2 Related Work

In this section, we present the related work on mmWave channel modeling and data driven TCP congestion control.

5.2.1 mmWave Channel

In [59] [60], research on the feasibility of using mmWave to provide wireless communication service are presented. In [51], researchers investigated the mmWave propagation loss, penetration loss, interference etc. The author provided a detailed statistical mmWave channel model based on outdoor measurement.

This model elaborates that mmWave system can provide an order of magnitude increase in capacity. The probabilities of outage and non-outage are provided. Coverage design technology and beam-forming scheme are discussed in [61] [62], which convince us that mmWave can be used for future wireless communication network design. Although mmWave channel can provide high capacity and low latency, it has a challenging issue: mmWave is sensitive to the obstructions like buildings, trees and even nearby pedestrian or vehicles. These obstructions may cause sudden, short and severe channel downgrade. How to increase the reaction speed to the channel fluctuations and fully utilize the channel capacity is the main issue for TCP congestion control protocol design. This chapter focuses on solving this problem from end user perspective.

5.2.2 Explicit Congestion Notification (ECN)

Legacy TCP congestion control protocols considered duplicate ACKs as indication of packet loss. With the addition of active queue management and ECN [63] to the network infrastructure, routers are capable to detect congestion before queue overflows. An additional Congestion Experienced (CE) byte is added to the IP header of the packet to support this function. Routers running RED queue management can mark the CE code point with certain probability when the average queue length is between minimal threshold and maximal threshold. When the average queue length exceeds the maximal threshold, upcoming packets' CE byte will be marked with probability 1. The packet with CE marked will be sent to the receiver. When the receiver received the packet, it will piggyback an ACK with CE marked to notify the sender that there is congestion in the router. No extra traffic will be generated to overload the network. The sender will reduce

the congestion window to avoid queue overflows and packet loss. Using ECN to detect congestion requires the participation of routers and waiting for receiver's feedback. We develop an end user congestion prediction scheme which utilize the idea of ECN without involving any network devices or waiting for any feedback.

5.2.3 Remy

Remy [64] is proposed by Keith Winstein in 2013. It designed congestion-control schemes based on prior knowledge of the network and the traffic model. It was the first computer generated congestion control protocol. A RemyCC tracks only three state variables of the end user:

- An exponentially-weighted moving average (EWMA) of the inter-arrival time between new ACKs received (ack_ewma).
- An EWMA of the time between TCP sender timestamps reflected in those ACKs (send_ewma).
- The ratio between the most recent Round Trip Time (RTT) and the minimum RTT seen during the current connection (rtt_ratio).

The algorithm does not require the support from any intermediate network devices. The end user can adjust its sending speed following the pre-generated algorithm based on the above mentioned data. This indicates that these three variables together might reflect the congestion state of the network.

Remy convinced us that designing a data driven congestion detection algorithm using end user data is possible. Since ECN gives the accurate information of whether there is congestion in the network or not, we decide to use end user data to predict ECN, thereby detect the congestion. The main contribution of this

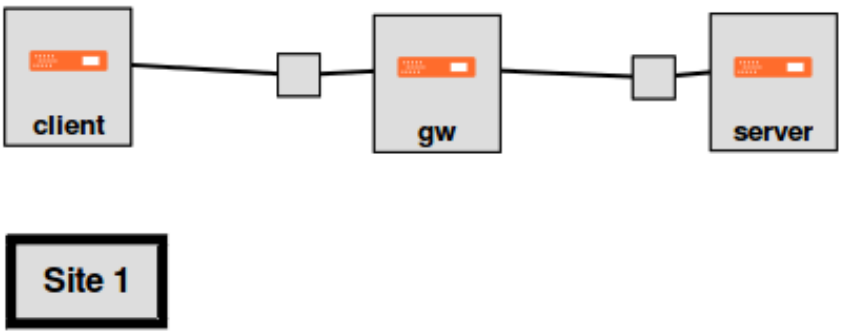

Figure 5.1: GENI Topology for Performance Evaluation

chapter is developing a data driven fast congestion detection algorithm (within one ACK inter-arrival time) using the end user data without support from receiver or router or other network devices.

5.3 Legacy TCP Performance on Mimic 5G Channel

Since Ethernet has similar capacity with mmWave channel, we use Ethernet with periodic on-off behavior to mimic the mmWave channel. On period means the channel is in the state of LOS while off period means the channel is NLOS state. We test two existing TCP congestion control protocol: NewReno and Cubic on the mimic 5G channel. In the GENI Portal, a three-node line topology with a server, a middle box and a client was set up as in Figure 5.1. Two different kinds of channel behavior are investigated: uniformly distributed on-off period and exponentially distributed on-off period. Congestion window size (CWND) and throughput are recorded to analyze the performance as in Figure 5.2, 5.3,

5.4 and 5.5. The channel capacity is set to be 1Gbps. Figure 5.2 illustrates the CWND of the sender when the off period is exponentially distributed with mean $10ms$, $100ms$, $1s$, while Figure 5.3 shows the corresponding throughput. Figure 5.4 and 5.5 presents the CWND and throughput when the off period is uniformly distributed between $0ms-10ms$, $0ms-100ms$, $0ms-1s$. In both cases, NewReno performance is deteriorated significantly due to the high frequency of off period. Figure 5.2, 5.4 showed every time off period happened, slow start will follow. The throughput is as low as 200Mbps, which is 1/5 of the full capacity. Compare with NewReno, from Figure 5.2, 5.4 we conclude that Cubic is more aggressive than NewReno. When channel recovers from off period to on period, Cubic will increase the CWND faster to utilize the channel capacity. When channel off time is at the level of 10ms, cubic even did not notice there is a connection lost. Instead, it behaves as congestion happened in the network and reduce the CWND. When the on time period is long enough as in the exponentially on-off period case, Cubic can still reach the upper limit of CWND and achieve full throughput as in Figure 5.3, while NewReno needs more time to recover. In the uniformly distributed on-off period case, the channel lost happened before Cubic fully recovered as in Figure 5.4. The CWND has a descending trend and the throughput decreases as time goes on. Based on the aforementioned observation, we conclude that even Cubic will not achieve high throughput if the channel switch between LOS (on) and NLOS (off) with a high frequency. Therefore, an aggressive congestion control protocol is necessary for the 5G network. In the following sections, we will focus on the initial step of design this protocol: developing a fast end-user congestion prediction scheme.

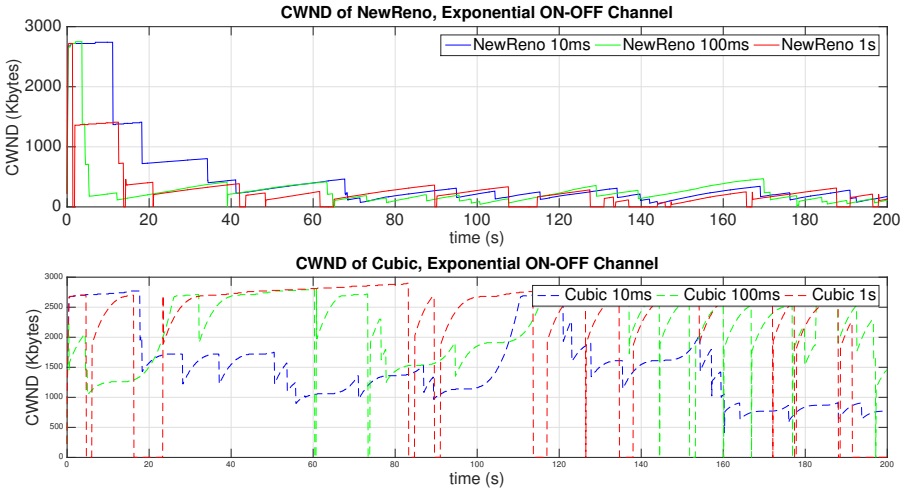

Figure 5.2: CWND dynamics given exponentially On-Off channel behavior

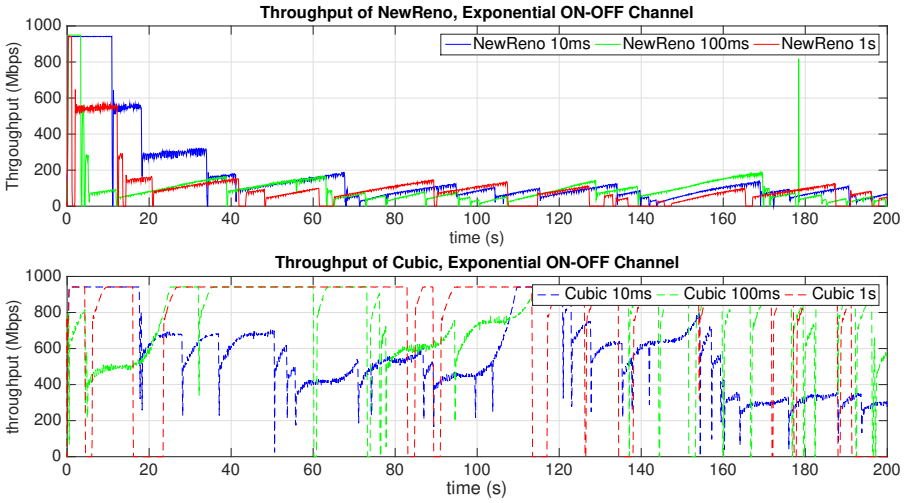

Figure 5.3: Throughput dynamics given exponentially On-Off channel behavior

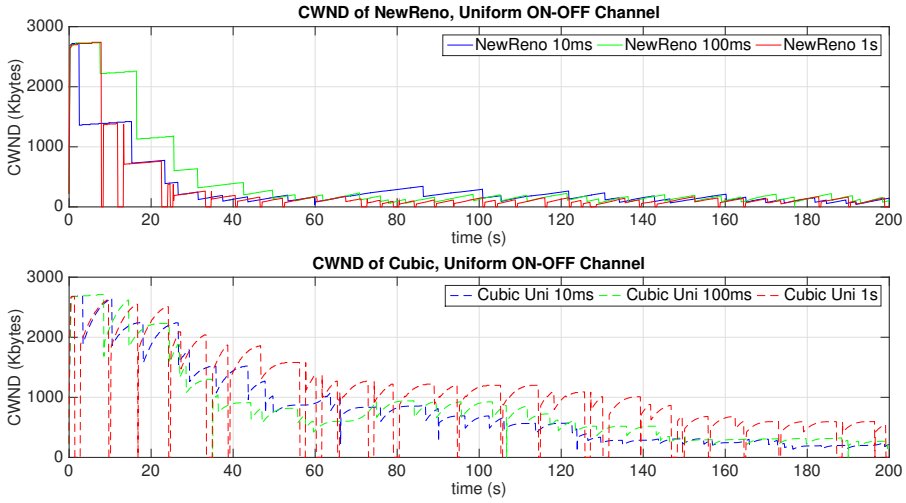

Figure 5.4: CWND dynamics given uniformly On-Off channel behavior

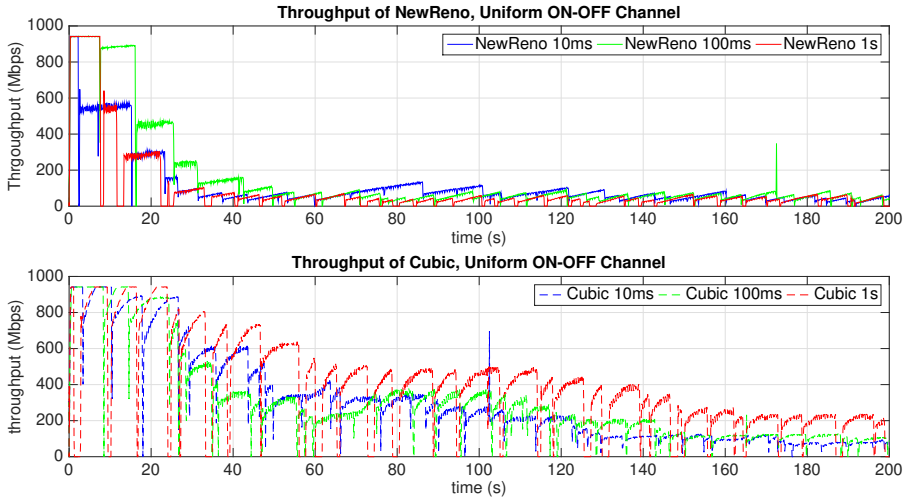

Figure 5.5: Throughput dynamics given uniformly On-Off channel behavior

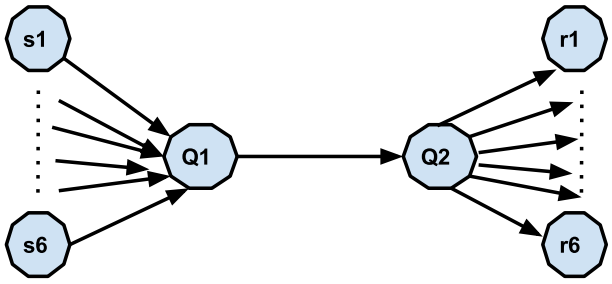

Figure 5.6: Network topology

5.4 Congestion Detection Algorithm

In this section, the design of the fast congestion detection algorithm is illustrated in detail. The principle idea is to predict the congestion in network within one inter-arrival time of ACKs from the end user data. The data which can be collected from end user includes packet sending time, ACK arriving time and the RTT calculated from these two time stamps. To collect these data for a particular network topology, we run simulations using discrete event based Network Simulator 2 (NS2).

5.4.1 Network Topology

A typical dumbbell model is presented and used in this section. The network topology is as in Figure 5.6. There are 6 TCP traffic senders and 6 receivers, sender si sends data to receiver ri through the bottleneck link $Q1 \rightarrow Q2$. Both $Q1$ and $Q2$ maintain a DropTail Queue. The queue limit is set to be the bandwidth-delay product to ensure the full utilization of the link capacity.

Congestion occurs when the occupied queue length exceeds the threshold T on the arriving of the incoming packet. To generate traces with congestion identifiers, we mark every packet as Congestion Experienced in the queue when the queue

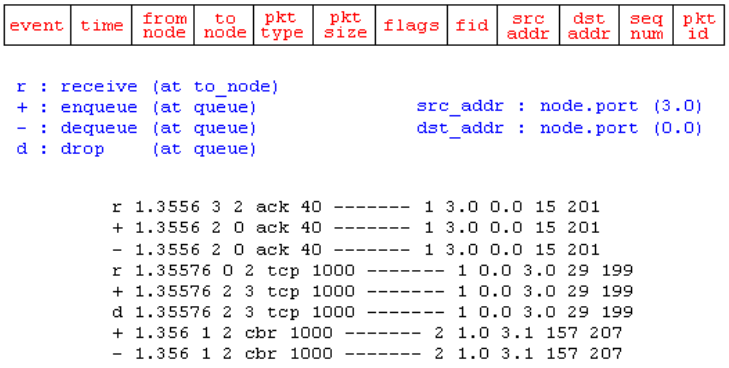

Figure 5.7: NS2 TCP trace format

length is greater than T. Typical NS2 TCP traces [65] are collected for future data processing as in Figure 5.7.

From the trace format we can identify the packet sending time, arriving time, packet size, unique ID, etc. Matching the packet unique ID, RTT can be calculated from packet sending time and corresponding ACK receiving time. For each unique packet, if congestion happens upon its arriving, the unique ID was recorded to be Congestion Experienced.

The drop tail queue behavior is displayed as follows. Figure 5.8 shows queue changes when traffic sources are running Cubic TCP with UDP competing traffic. In this case, when queue length is greater than 450 packets, the incoming packets will be marked as congestion experienced.

5.4.2 Data Collection

Without losing generality of the analysis, we simulated several different traffic scenarios to collect end user data. We investigated following scenarios:

- Scenario 1: All traffic sources are running TCP NewReno with stationary bottleneck link capacity.

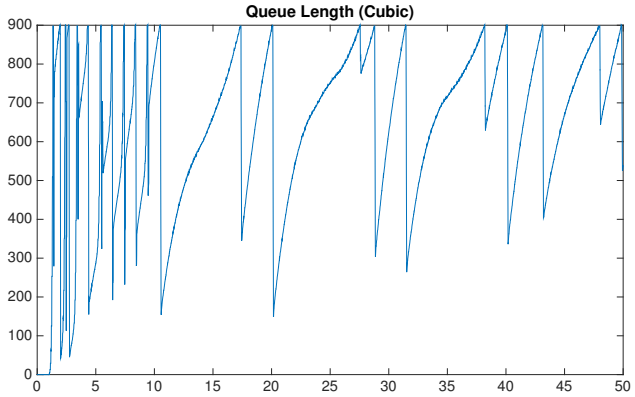

Figure 5.8: Queue length dynamics (Cubic)

- Scenario 2: All traffic sources are running TCP Cubic with stationary bottleneck link capacity.
- Scenario 3: One half of traffic sources are running TCP NewReno while the other half are running UDP with stationary bottleneck link capacity.
- Scenario 4: One half of traffic sources are running TCP Cubic while the other half are running UDP with stationary bottleneck link capacity.
- Scenario 5: Repeat scenario 1 and 2 for a periodically On-Off bottleneck link.

The bottleneck link for those scenarios is link $Q1 \rightarrow Q2$. Detailed simulation parameters are shown in TABLE 5.1.

The data which is available from end user are packet sending time t_s and ACK receiving time t_r. From these two timestamps, we can calculate packet sending interval $T_{s_i} = t_{s_i} - t_{s_{i-1}}$, ACK inter-arrival time $T_{r_i} = t_{r_i} - t_{r_{i-1}}$ and Round Trip Time (RTT) $RTT_i = t_{s_i} - t_{r_i}$. From the above three available time intervals, we develop 5 features that are used in the congestion prediction algorithm.

- Sending time interval between two consecutive packets T_{s_i}.

Table 5.1: Simulation Parameters

Access Link Capacity	1Gbps
BottleNeck Link Capacity	1Gbps
Access Link Delay	5ms
BottleNeck Link Delay	10ms
Queue Capacity	Delay-Bandwidth Product

- Receiving time interval between two consecutive ACKs T_{r_i}.
- An exponentially-weighted moving average (EWMA) of T_{s_i} (send_ewma).
- An EWMA of T_{r_i} (ack_ewma).
- The ratio between the most recent RTT and the minimum RTT seen during the entire connection period (rtt_ratio).

These above five features constructed the feature set to train the machine learning algorithm and predict the congestion.

5.4.3 Congestion Prediction

Every sample of the data collected from above five scenarios includes five features and a congestion identifier: Virtual ECN (0 stands for non congestion experienced, 1 stands for congestion experienced). The problem to be solved is a binary classification problem: train an algorithm to classify the sample data into two categories: congestion experienced and no congestion. First we run Logistic Regression, a popular binary classification algorithm, is used to train the sample data and predict congestion. The area under ROC curve is 0.89 as shown in Figure. 5.9. The performance of Logistic Regression is good $(0.80 - 0.90)$. The decision boundary is $-2.31936102 * f_1 - 33.36046689 * f_2 - 12.65365902 * f_3 -$

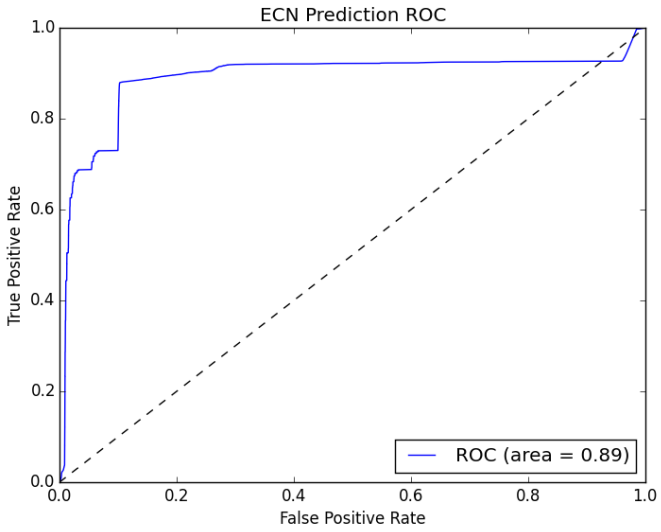

Figure 5.9: ROC curve of Logistic Regression classifier

$15.29961927 * f_4 + 2.0344486 * f_5 - 2.69202498 = 0$, where f_1, f_2, f_3, f_4, f_5 are the five corresponding features.

Next we applied Decision Tree algorithm and regulated the maximum depth of the tree to be 5 and the minimum samples in each leaf node to be 10000 to avoid overfitting. Figure. 5.10a gives the ROC curve of Decision Tree Classifier. The area under ROC curve is 0.98. This indicates excellent $(0.90 - 1)$ prediction result. The feature importance are given as [0.011703, 0.00085, 0.000000, 0.03985, 0.94760] for [T_{s_i}, T_{r_i}, send_ewma, receive_ewma, rtt_ratio], from which we can conclude that rtt_ratio is the most important feature to predict congestion.

Further we changed the maximum depth to 3 and minimum samples of each leaf node to 100000, the ROC is displayed in Figure. 5.10b. The feature importance becomes [0, 0, 0, 0, 1]. This indicates the decision tree is doing the binary classification merely based on rtt_ratio. All other features are not contributed to the binary classification process. The decision tree is shown in Figure. 5.11. In Figure. 5.11, X[4] is rtt_ratio, the first layer is classified by this feature. The cu-

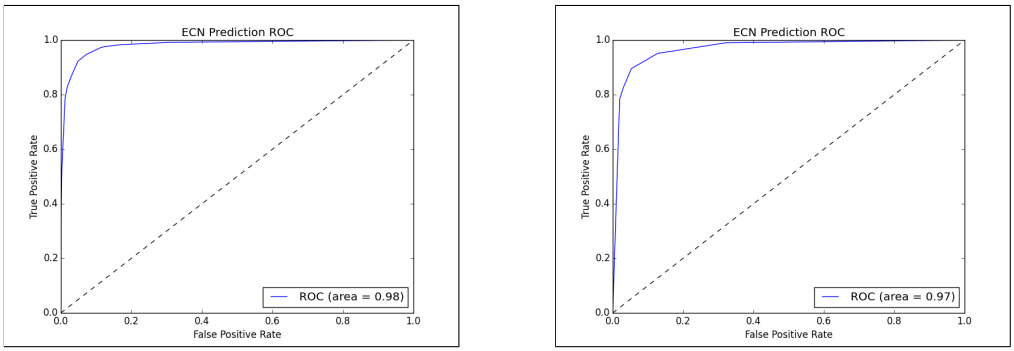

(a) max_depth = 5, min_samples_leaf = 10000

(b) max_depth = 3, min_samples_leaf = 100000

Figure 5.10: ROC curve of Decision Tree classifier

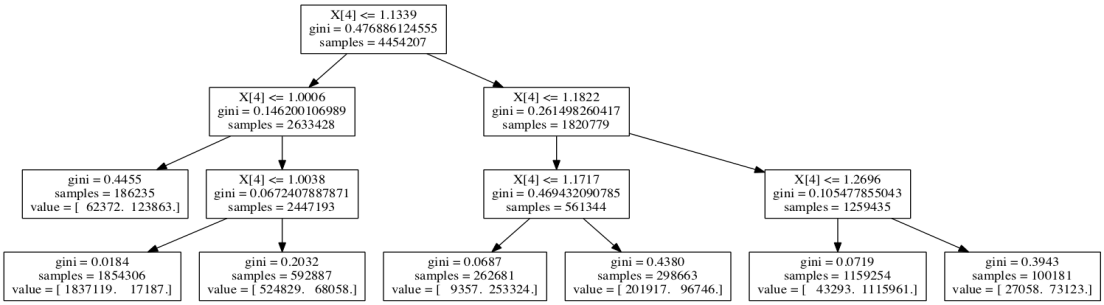

Figure 5.11: Decision Tree (max_depth = 3, min_samples_leaf = 100000)

mulative density function (CDF) of rtt_ratio is given in Figure. 5.12a. The blue line is the CDF curve of rtt_ratio when congestion is experienced while the red line is when congestion is not experienced. Take 1.2 as an example, the probability of rtt_ratio to be less than 1.13 is 82% when there is no congestion. However, that probability is approximately 0% when congestion experienced. This is consistent with the result of feature importance generated from Decision Tree algorithm.

The above results are generated from a network with fixed propagation delay. To learn how this prediction algorithm works when network condition changes, we investigated Scenario 1 and 2 with variations of propagation delay. We simulated networks with access delay and queue capacity as in TABLE 5.2. The Logistic Regression algorithm generated the ROC curve as in Figure. 5.13a. The area under

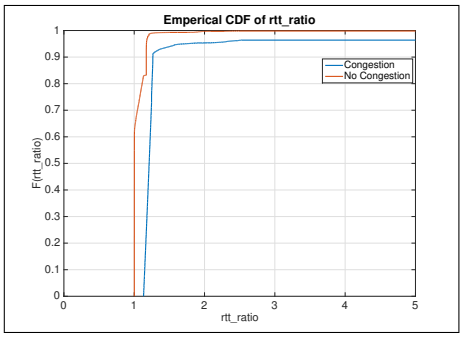

(a) CDF of rtt_ratio with same propagation delay

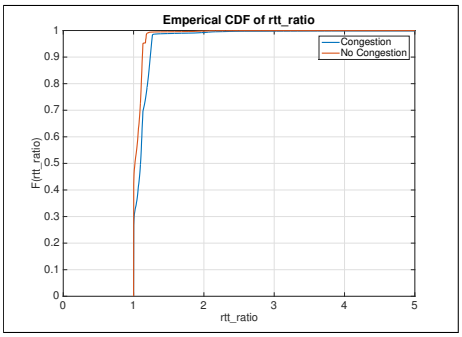

(b) CDF of rtt_ratio with different propagation delay

Figure 5.12: CDF of rtt_ratio

Table 5.2: Simulation Parameters

Access Link Delay	5ms, 10ms, 20ms
BottleNeck Link Delay	10ms, 20ms, 40ms
Queue Capacity	Delay-Bandwidth Product

ROC curve is 0.654497, which indicates poor performance $(0.60-0.70)$. The decision boundary is $-0.46605323*f_1-7.33485574*f_2-0.34620622*f_3-1.41154115*f_4+5.20171832*f_5-5.53557771=0$. The coefficient of each feature follows the same pattern as before. Decision Tree classifier is then applied to the collected dataset. The ROC curve is as in Figure. 5.13b. The area under ROC curve is 0.701188, which is on the boundary of poor performance. The feature importance is [0.000955787581, 0.000389816495, 0.00489484823, 0.0636899225, 0.930069625]. This is consistent with the previous result that rtt_ratio is the most important feature. Those two figures indicate that when network condition changes, the predictability of congestion from the aforementioned five features decreases. Figure. 5.12b shows the CDF of rtt_ratio with different link propagation delay. The figure indicates near 30% overlap of the CDF curve of Congestion Experience packet and No Congestion packet. This again verifies the prediction results.

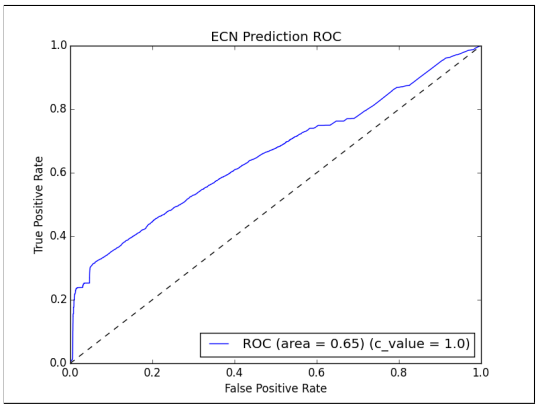

(a) ROC curve of Logistic Regression classifier with different propagation delay

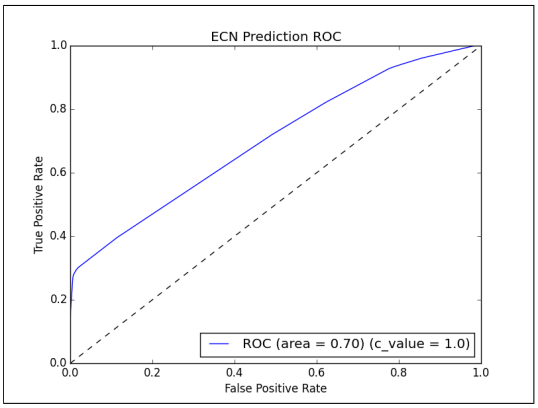

(b) ROC curve of Decision Tree classifier with different propagation delay

Figure 5.13: ROC curves with different propogation delay

5.5 Chapter Summary

In this chapter, we proposed a data driven machine learning congestion detection algorithm. Datasets are collected using NS2 for a dumbbell model with five different traffic scenarios. Five features are formatted from end user data. When the network condition is not changing, which means the propagation delay of each link is stable, our algorithm can detect congestion with high precision from the five features. In contrast, if the network condition changes, the algorithm fails to work. In both cases, rtt_ratio is the most important feature to predict congestion. Other four features are less useful when doing the binary classification. The area under ROC curve is consistent with the CDF of rtt_ratio. For stable network, a fast reacting congestion control algorithm can be designed based on our congestion detection algorithm for 5G mmWave communication network.

Chapter 6

Conclusion

Appendices

Appendix A

A.1 Title of Appendix A

Appendix B

B.1 Title of Appendix B

Bibliography

[1] C. V. N. Index, "Global mobile data traffic forecast update, 2012-2017," *Cisco white paper*, 2013.

[2] P. Cerwall and S. Bergqvist, "Ericsson traffic and market data report [r]," *Ericsson, Stockholm, Sweden, Nov*, 2011.

[3] F. Pujol, "?mobile traffic forecasts 2010-2020 & offloading solutions," *IDATE Consulting and Research, May*, vol. 15, 2011.

[4] F. Khan and Z. Pi, "mmwave mobile broadband (mmb): Unleashing the 3–300ghz spectrum," in *Sarnoff Symposium, 2011 34th IEEE*. IEEE, 2011, pp. 1–6.

[5] Z. Pi and F. Khan, "An introduction to millimeter-wave mobile broadband systems," *IEEE Communications Magazine*, vol. 49, no. 6, 2011.

[6] T. S. Rappaport, J. N. Murdock, and F. Gutierrez, "State of the art in 60-ghz integrated circuits and systems for wireless communications," *Proceedings of the IEEE*, vol. 99, no. 8, pp. 1390–1436, 2011.

[7] P. Pietraski, D. Britz, A. Roy, R. Pragada, and G. Charlton, "Millimeter wave and terahertz communications: Feasibility and challenges," *ZTE Communications*, vol. 10, no. 4, pp. 3–12, 2012.

[8] S. Rangan, T. S. Rappaport, and E. Erkip, "Millimeter-wave cellular wireless networks: Potentials and challenges," *Proceedings of the IEEE*, vol. 102, no. 3, pp. 366–385, 2014.

[9] C. H. Doan, S. Emami, D. A. Sobel, A. M. Niknejad, and R. W. Brodersen, "Design considerations for 60 ghz cmos radios," *IEEE Communications Magazine*, vol. 42, no. 12, pp. 132–140, 2004.

[10] Y. P. Zhang and D. Liu, "Antenna-on-chip and antenna-in-package solutions to highly integrated millimeter-wave devices for wireless communications," *IEEE Transactions on Antennas and Propagation*, vol. 57, no. 10, pp. 2830–2841, 2009.

[11] F. Gutierrez, S. Agarwal, K. Parrish, and T. S. Rappaport, "On-chip integrated antenna structures in cmos for 60 ghz wpan systems," *IEEE Journal on Selected Areas in Communications*, vol. 27, no. 8, 2009.

[12] S. Rajagopal, S. Abu-Surra, Z. Pi, and F. Khan, "Antenna array design for multi-gbps mmwave mobile broadband communication," in *Global Telecommunications Conference (GLOBECOM 2011), 2011 IEEE*. IEEE, 2011, pp. 1–6.

[13] A. Goldsmith, *Wireless Communications*. Cambridge University Press, 2005.

[14] V. Graziano, "Propagation correlations at 900 MHz," *Vehicular Technology, IEEE Transactions on*, vol. 27, no. 4, pp. 182–189, 1978.

[15] M. Marsan, G. Hess, and S. Gilbert, "Shadowing variability in an urban land mobile environment at 900 mhz," *Electronics Letters*, vol. 26, no. 10, pp. 646–648, 1990.

[16] J. C. Liberti and T. S. Rappaport, "Statistics of shadowing in indoor radio channels at 900 and 1900 mhz," in *Military Communications Conference, 1992. MILCOM'92, Conference Record. Communications-Fusing Command, Control and Intelligence., IEEE.* IEEE, 1992, pp. 1066–1070.

[17] S. S. Szyszkowicz, H. Yanikomeroglu, and J. S. Thompson, "On the feasibility of wireless shadowing correlation models," *Vehicular Technology, IEEE Transactions on*, vol. 59, no. 9, pp. 4222–4236, 2010.

[18] D. Kitchener, M. Naden, W. Tong, P. Zhu, G. Senarnath, H. Zhang, D. Steer, and D. Yu, "Correlated lognormal shadowing model," *San Diego, CA, IEEE*, vol. 802, 2006.

[19] S. S. Szyszkowicz, "Interference from large wireless networks under correlated shadowing," Ph.D. dissertation, Carleton University, 2011.

[20] S. S. Panwar, *TCP/IP Essentials: A Lab-Based Approach.* Cambridge University Press, 2004.

[21] T. S. Rappaport, *Wireless Communications: Principles and Practice.* Prentice Hall PTR New Jersey, 1996.

[22] F. Fabbri and R. Verdone, "The impact of correlated channel fluctuations on the connectivity of wireless ad-hoc networks," in *Vehicular Technology Conference, 2009. VTC Spring 2009. IEEE 69th.* IEEE, 2009, pp. 1–5.

[23] N. Patwari and P. Agrawal, "Effects of correlated shadowing: Connectivity, localization, and rf tomography," in *Information Processing in Sensor Networks, 2008. IPSN'08. International Conference on.* IEEE, 2008, pp. 82–93.

[24] M.-K. Chang and S.-Y. Lee, "Performance analysis of cooperative communication system with hierarchical modulation over rayleigh fading channel," *Wireless Communications, IEEE Transactions on*, vol. 8, no. 6, pp. 2848–2852, 2009.

[25] Y. Lee and M.-H. Tsai, "Performance of decode-and-forward cooperative communications over nakagami-fading channels," *Vehicular Technology, IEEE Transactions on*, vol. 58, no. 3, pp. 1218–1228, 2009.

[26] R. Madan, N. B. Mehta, A. F. Molisch, and J. Zhang, "Energy-efficient cooperative relaying over fading channels with simple relay selection," *Wireless Communications, IEEE Transactions on*, vol. 7, no. 8, pp. 3013–3025, 2008.

[27] V. Emamian, P. Anghel, and M. Kaveh, "Multi-user spatial diversity in a shadow-fading environment," in *Vehicular Technology Conference, 2002. Proceedings. VTC 2002-Fall. 2002 IEEE 56th*, vol. 1. IEEE, 2002, pp. 573–576.

[28] B. Kasiri, M. Naderi, and B. Abolhassani, "A new realistic relay selection method based on correlated shadowing for multihop cellular networks," in *Computer and Electrical Engineering, 2008. ICCEE 2008. International Conference on.* IEEE, 2008, pp. 669–673.

[29] S. Park and W. Stark, "Opportunistic relaying in multipath and slow fading channel: Relay selection and optimal relay selection period," in *Military Communications Conference, 2011-MILCOM 2011.* IEEE, 2011, pp. 661–666.

[30] A. Bletsas, H. Shin, M. Z. Win *et al.*, "Outage-optimal cooperative communications with regenerative relays," in *Information Sciences and Systems, 2006 40th Annual Conference on.* IEEE, 2006, pp. 632–637.

[31] N. Zlatanov, R. Schober, Z. Hadzi-Velkov, and G. Karagiannidis, "Average outage and non-outage duration of selective decode-and-forward relaying," in *Information Theory (CWIT), 2011 12th Canadian Workshop on*. IEEE, 2011, pp. 94–97.

[32] D. Kaltakis, M. A. Imran, and R. Hoshyar, "Uplink capacity with correlated lognormal shadow fading," in *Vehicular Technology Conference, 2009. VTC Spring 2009. IEEE 69th*. IEEE, 2009, pp. 1–5.

[33] A. Nosratinia, T. E. Hunter, and A. Hedayat, "Cooperative communication in wireless networks," *Communications Magazine, IEEE*, vol. 42, no. 10, pp. 74–80, 2004.

[34] S. Saunders and A. Aragón-Zavala, *Antennas and propagation for wireless communication systems*. John Wiley & Sons, 2007.

[35] M. Gudmundson, "Correlation model for shadow fading in mobile radio systems," *Electronics Letters*, vol. 27, no. 23, pp. 2145–2146, 1991.

[36] Y. Zhang, J. Zhang, D. Dong, X. Nie, G. Liu, and P. Zhang, "A novel spatial autocorrelation model of shadow fading in urban macro environments," in *Global Telecommunications Conference, 2008. IEEE GLOBECOM 2008. IEEE*. IEEE, 2008, pp. 1–5.

[37] T. B. Sorensen, "Correlation model for slow fading in a small urban macro cell," in *Personal, Indoor and Mobile Radio Communications, 1998. The Ninth IEEE International Symposium on*, vol. 3. IEEE, 1998, pp. 1161–1165.

[38] J. Weitzen and T. J. Lowe, "Measurement of angular and distance correlation properties of log-normal shadowing at 1900 MHz and its application to design of PCS systems," *Vehicular Technology, IEEE Transactions on*, vol. 51, no. 2, pp. 265–273, 2002.

[39] H. L. Bertoni, *Radio Propagation for Modern Wireless Systems*. Pearson Education, 1999.

[40] W. W.-S. Wei, *Time Series Analysis*. Addison-Wesley Publ, 1994.

[41] A. Papoulis and S. U. Pillai, *Probability, Random Variables, and Stochastic Processes*. McGraw-Hill Higher Education, 2002.

[42] A. A. Abu-Dayya and N. C. Beaulieu, "Outage probabilities of cellular mobile radio systems with multiple nakagami interferers," *Vehicular Technology, IEEE Transactions on*, vol. 40, no. 4, pp. 757–768, 1991.

[43] I. Petrovic, M. Stefanovic, P. Spalevic, S. R. Panic, and D. Stefanovic, "Outage analysis of selection diversity over rayleigh fading channels with multiple co-channel interferers," *Telecommunication Systems*, vol. 52, no. 1, pp. 39–50, 2013.

[44] V. Emamian, "Outage analysis of a multi-user spatial diversity system in a shadow-fade propagating channel," *British Journal of Applied Science & Technology*, vol. 4, no. 1, p. 40, 2014.

[45] M. Vural, G. K. Kurt, and C. Schneider, "The effect of shadow fading distributions on outage probability and coverage area," in *Vehicular Technology Conference (VTC Spring), 2015 IEEE 81st*. IEEE, 2015, pp. 1–6.

[46] T. Lu, P. Liu, and S. S. Panwar, "How long before i regain my signal?" in *Information Sciences and Systems (CISS), 2015 49th Annual Conference on*. IEEE, 2015, pp. 1–5.

[47] T. Lu, P. Liu, and S. Panwar, "Shining a light into the darkness: How cooperative relay communication mitigates correlated shadow fading," in *Vehicular Technology Conference (VTC Spring), 2015 IEEE 81st*. IEEE, 2015, pp. 1–7.

[48] J. G. Andrews, F. Baccelli, and R. K. Ganti, "A tractable approach to coverage and rate in cellular networks," *Communications, IEEE Transactions on*, vol. 59, no. 11, pp. 3122–3134, 2011.

[49] C. S. Chen, V. M. Nguyen, and L. Thomas, "On small cell network deployment: A comparative study of random and grid topologies," in *Vehicular Technology Conference (VTC Fall), 2012 IEEE*. IEEE, 2012, pp. 1–5.

[50] S. Kumar, "Approximate outage probability and capacity for-shadowed fading," *Wireless Communications Letters, IEEE*, vol. 4, no. 3, pp. 301–304, 2015.

[51] M. R. Akdeniz, Y. Liu, M. K. Samimi, S. Sun, S. Rangan, T. S. Rappaport, and E. Erkip, "Millimeter wave channel modeling and cellular capacity evaluation," *Selected Areas in Communications, IEEE Journal on*, vol. 32, no. 6, pp. 1164–1179, 2014.

[52] T. Bai and R. W. Heath, "Coverage and rate analysis for millimeter-wave cellular networks," *Wireless Communications, IEEE Transactions on*, vol. 14, no. 2, pp. 1100–1114, 2015.

[53] J. Lu, D. Steinbach, P. Cabrol, and P. Pietraski, "Modeling the impact of human blockers in millimeter wave radio links," *ZTE Commun. Mag*, vol. 10, no. 4, pp. 23–28, 2012.

[54] H. Zhao, R. Mayzus, S. Sun, M. Samimi, J. K. Schulz, Y. Azar, K. Wang, G. N. Wong, F. Gutierrez, and T. S. Rappaport, "28 ghz millimeter wave cellular communication measurements for reflection and penetration loss in and around buildings in new york city," in *Communications (ICC), 2013 IEEE International Conference on.* IEEE, 2013, pp. 5163–5167.

[55] A. V. Alejos, M. G. Sánchez, and I. Cuiñas, "Measurement and analysis of propagation mechanisms at 40 ghz: Viability of site shielding forced by obstacles," *Vehicular Technology, IEEE Transactions on*, vol. 57, no. 6, pp. 3369–3380, 2008.

[56] L. Xu, K. Harfoush, and I. Rhee, "Binary increase congestion control (bic) for fast long-distance networks," in *INFOCOM 2004. Twenty-third AnnualJoint Conference of the IEEE Computer and Communications Societies*, vol. 4. IEEE, 2004, pp. 2514–2524.

[57] S. Ha, I. Rhee, and L. Xu, "Cubic: a new tcp-friendly high-speed tcp variant," *ACM SIGOPS Operating Systems Review*, vol. 42, no. 5, pp. 64–74, 2008.

[58] K. Tan, J. Song, Q. Zhang, and M. Sridharan, "A compound tcp approach for high-speed and long distance networks," in *Proceedings-IEEE INFOCOM*, 2006.

[59] Y. Niu, Y. Li, D. Jin, L. Su, and A. V. Vasilakos, "A survey of millimeter wave communications (mmwave) for 5g: opportunities and challenges," *Wireless Networks*, pp. 1–20, 2015.

[60] T. S. Rappaport, S. Sun, R. Mayzus, H. Zhao, Y. Azar, K. Wang, G. N. Wong, J. K. Schulz, M. Samimi, and F. Gutierrez, "Millimeter wave mobile communications for 5g cellular: It will work!" *Access, IEEE*, vol. 1, pp. 335–349, 2013.

[61] S. Sun, G. R. MacCartney, M. K. Samimi, S. Nie, and T. S. Rappaport, "Millimeter wave multi-beam antenna combining for 5g cellular link improvement in new york city," in *Communications (ICC), 2014 IEEE International Conference on*. IEEE, 2014, pp. 5468–5473.

[62] W. Roh, J.-Y. Seol, J. Park, B. Lee, J. Lee, Y. Kim, J. Cho, K. Cheun, and F. Aryanfar, "Millimeter-wave beamforming as an enabling technology for 5g cellular communications: theoretical feasibility and prototype results," *Communications Magazine, IEEE*, vol. 52, no. 2, pp. 106–113, 2014.

[63] K. Ramakrishnan, S. Floyd, and D. Black, "Rfc 3168," *The addition of Explicit Congestion Notification (ECN) to IP. The Internet Society*, 2001.

[64] K. Winstein and H. Balakrishnan, "Tcp ex machina: Computer-generated congestion control," in *ACM SIGCOMM Computer Communication Review*, vol. 43, no. 4. ACM, 2013, pp. 123–134.

[65] "Trace analysis example," http://nile.wpi.edu/NS/analysis.html, accessed: 2016-4-5.